THE ASTROPHYSICAL JOURNAL, 492:1–28, 1998 January 1


# RECONSTRUCTING THE SPECTRUM OF THE PREGALACTIC DENSITY FIELD FROM ASTRONOMICAL DATA

A. KASHLINSKY[1]
Hughes STX, Code 685, Goddard Space Flight Center, Greenbelt, MD 20771; NORDITA, Blegdamsvej 17, DK-2100 Copenhagen 0, Denmark; and Theoretical Astrophysics Center, Juliane Maries Vej 30, DK-2100 Copenhagen 0, Denmark
*Received 1997 April 25; accepted 1997 August 6*

## ABSTRACT

In this paper we evaluate the spectrum of the pregalactic density field on scales $1\ h^{-1}$ Mpc $< r < 100\ h^{-1}$ Mpc from a variety of astronomical data. We start with the APM data on the projected angular correlation function, $w(\theta)$, in six narrow magnitude bins and check whether possible evolutionary effects can affect inversion of the $w(\theta)$ data in terms of the underlying power spectrum. This is done by normalizing to the angular correlation function on small scales where the underlying three-dimensional galaxy correlation function, $\xi(r)$ is known. Using the Automatic Plate Measuring Facility (APM) data in narrow magnitude bins allows us to test the various fits to the APM data power spectrum more accurately. We find that for linear scales $r > 10\ h^{-1}$ Mpc, the Baugh & Efstathiou spectrum of galaxy distribution gives the best fit to the data at all depths. Fitting power spectra of cold dark matter (CDM) models to the data at all depths requires $\Omega h = 0.2$ if the primordial index $n = 1$ and $\Omega h = 0.3$ if the spectrum is tilted with $n = 0.7$. Next we compare the peculiar velocity field predicted by the APM spectrum of galaxy (light) distribution with the actual velocity data. The two fields are consistent, and the comparison suggests that the bias factor is scale independent with $\Omega^{0.6}/b \simeq (0.2–0.4)$. These steps enable us to fix the pregalactic mass-density field on scales between 10 and $\sim 100\ h^{-1}$ Mpc. The next data set we use to determine the pregalactic density field comes from the cluster correlation data. We calculate in detail the amplification of the cluster correlation function due to gravitational clustering and use the data on both the slope of the cluster correlation function and its amplitude-richness dependence. Cluster masses are normalized using the Coma Cluster. We find that no CDM model can fit all three data sets: APM data on $w(\theta)$, the data on cluster correlation function, and the data on the latter's amplitude-richness dependence. Next we show that the data on the amplitude-richness dependence can be used directly to obtain the spectrum of the pregalactic density field. Applying the method to the data, we recover the density field on scales between 5 and 25 $h^{-1}$ Mpc whose slope is in good agreement with the APM data on the same scales. Requiring the two amplitudes to coincide fixes the value of $\Omega$ to be 0.25–0.3 in agreement with observations of the dynamics of the Coma Cluster. We then use the data on high-$z$ objects to constrain the small-part, (1–5) $h^{-1}$ Mpc of the pregalactic density field. We argue that the data at high redshifts require more power than given by CDM models normalized to the APM and cluster data. Then we reconstruct the pregalactic density field out of which modern-day galaxies have formed. We use the data on blue absolute luminosities, the fundamental plane relations, and the latest X-ray data on the halo velocity dispersion. From this we recover the pregalactic density field on comoving scales between 1 and 5 $h^{-1}$ Mpc, which is in reasonable agreement with the simple power-law extrapolation from the larger scales.

*Subject headings:* cosmology: dark matter — cosmology: theory — galaxies: formation — large-scale structure of universe

## 1. INTRODUCTION

The origin of structure in the universe is one of the most outstanding problems in modern cosmology. In the gravitational instability picture, it is assumed that structures in the universe formed by gravitational growth of small density fluctuations seeded at some early epoch of the universe evolution. The *COBE* discovery of the microwave background anisotropies (Smoot et al. 1992, Bennett et al. 1996) proved convincingly that density fluctuations were already present at $z \simeq 1000$. It is then reasonable to assume that these were indeed the seeds of the density field that were to lead to present-day structures. Following the *COBE* discovery of the large-scale structure at $z \sim 1000$, it is therefore even more imperative to try to reconstruct the pregalactic density field on scales and at epochs inaccessible to the microwave background measurements.

The spectrum of the density field determines the epoch and the order of galaxy and structure formation. Its normalization point is fixed by observations that show that fluctuations in galaxy counts today at $z = 0$ have unity amplitude on scale $r_8 = 8\ h^{-1}$ Mpc. Given this amplitude at $r_8$, or mass scale $\sim 10^{15}\ M_\odot$, and the slope of the spectrum, one can predict when and on what scales the first objects in the universe began to collapse. The converse is also true. Similarly, on scales greater than $r_8$ where the density field is still in linear regime, the various properties of galaxy and cluster distribution can be used to determine the spectrum of the density field on scales currently inaccessible to spaceborne microwave background measurements.

[1] kashlinsky@stars.gsfc.nasa.gov.

On a theoretical level, the density field is assumed to have been seeded at some early epoch in the evolution of the universe. The most popular of such mechanisms involves inflationary cosmology with cold dark matter (CDM) contributing most of the mass in the universe. Various discussions have also concentrated on the density fluctuations seeded by topological defects, such as strings and textures, that can be produced naturally during early phase transitions. Another possibility is the empirical approach, not necessarily motivated by the current ideas from high-energy physics, whereby one deduces the properties of the early universe from the present data, instead of "predicting" what the properties of the present-day universe should be.

The density field at some early time can be characterized by both its spatial and its Fourier components, which are related via $\delta(x) = (2\pi)^{-3} \int \delta_k \exp(-ik \cdot x) d^3k$. If one assumes the density field to be a random variable, one can describe its statistical properties via the moments of its probability distribution. Assuming an overall spherical symmetry, the correlation function of the field is defined as the generalized scalar product $\xi(r) = \langle \delta(x + r)\delta(x) \rangle$. The power spectrum is defined as $P(k) = \langle | \delta_k |^2 \rangle$, where the average is performed over all phases. The correlation function and the power spectrum represent a pair of three-dimensional Fourier transforms. In addition, the mean square fluctuation over a sphere of volume $V$ containing mass $M$ is related to $\xi(r)$ via $\Delta^2(M) = \langle \{ [\int \delta(x) dV]/V \}^2 \rangle = [\int \xi(r) dV]/V$. If the phases of $\delta_k$ are random, the distribution of the density field is Gaussian, and the correlation function (or its Fourier transform) uniquely describes all properties of the density distribution. The central limit theorem ensures that the Gaussian distribution is reached in most inflationary mechanisms for generating energy density fluctuations. In models with topological defects, however, the density field is not Gaussian and, in addition to $\xi(r)$ is determined by higher moments of the probability distribution.

Enough data have now been accumulated over a large range of scales to strongly constrain the models, on the one hand, and on the other to attempt to determine the spectrum of the pregalactic density field independently of theoretical prejudices. This is the aim of this article, where we analyze the various data to show that the data lead to a consistent and unique density field in the pregalactic universe.

When using the data derived from galaxy catalogs, one determines the distribution of light, whereas, in order to understand the physics of galaxy formation and the early universe, one needs to determine the distribution of mass. Therefore, one has to introduce the biasing factor which determines how the two are related to each other. The most common assumption is that of linear biasing, $\delta_{\rm light} \propto \delta_{\rm mass}$, although more complex and complicated biasing schemes can be considered. Therefore, before we proceed to the main results of the paper, we address the reliability of the general assumption of light tracing mass by comparing the velocity field predicted by the galaxy correlation function data with peculiar velocities in the Great Attractor region.

The plan of the paper is as follows: In § 2 we briefly define the CDM models that we will test against the data in the paper and discuss the microwave background (*COBE* Differential Microwave Radiometer [DMR]) constraints on the very large scale part of the density field, where it is likely that the power spectrum has preserved its original slope. In § 3 we analyze the data from the APM survey divided into narrow magnitude bins ($\Delta m \simeq 0.5$) which contain galaxies at the same evolutionary stages. In this way, we establish if significant galaxy evolution effects could affect determination of the spectrum of the density field from the projected APM data. Following this, we discuss various fits to the APM data and conclude that they all give essentially the same field of light (galaxy) distribution on linear scales, $r > r_8$. The data in the narrow magnitude bins, however, set somewhat stronger limits on CDM models than used before. In § 4 we elaborate on a method to interrelate the data on the galaxy correlation function from both APM and CfA catalogs with that on peculiar velocities. This establishes whether the light traces light and the constraints both data sets suggest for $\Omega$ and the bias factor. Thus we determine the spectrum of the pregalactic mass density field and its correlation function on scales (10–100) $h^{-1}$ Mpc. In § 5 we calculate the amplification in the cluster correlation function due to gravitational clustering of density fluctuations. We then use the data both on the spatial slope of the cluster correlation function and on its richness-amplitude dependence in order to set further constraints on the CDM models. We devise a method to invert the richness-correlation amplitude dependence of clusters of galaxies in order to obtain directly the spectrum of the pregalactic density field on scales (5–20) $h^{-1}$ Mpc. In § 6 we provide a comparison of the density field deduced independently from the APM catalog and that deduced from the cluster correlation data in order to constrain $\Omega$ by requiring that the two match on the same scales. In § 7 we discuss the limits on the small-scale part of the pregalactic density field from the data on the existence and ages of high-$z$ galaxies and clusters. We also reconstruct the pregalactic density field from the data on the fundamental plane of modern-day (elliptical) galaxies, their absolute photometry, and the dynamics of their halos from the recent X-ray observations. In § 8 we reconstruct the *pregalactic* density field over two decades in linear scale, $\sim$(1–100) $h^{-1}$ Mpc. Conclusions are summarized in § 9.

## 2. THE EARLY UNIVERSE *ANSÄTZ*: MICROWAVE BACKGROUND AND VERY LARGE SCALES

Because of its elegance and simplicity, inflation is probably the most popular of the current theories for the origin of structure in the universe. The density field in the inflationary picture originates from quantum energy fluctuations generated during the slow rollover of the inflation field during this era. Exponential expansion of the underlying spacetime during inflation ensures that the fluctuations are seeded by normal causal processes on scales well in excess of the current particle horizon of $\sim 6000\ h^{-1}$ Mpc. In its simplest and most natural form, inflation leads to Gaussian adiabatic density fluctuations with the initial power spectrum, which is scale-free and has the Harrison-Zeldovich slope, $P_i(k) \propto k^n$ with $n = 1$. In conjunction with the *COBE* observations, inflationary models generally require a flat universe (Kashlinsky, Tkachev & Frieman 1994), while big bang nucleosynthesis implies a small baryon density (e.g., Walker et al. 1991). Thus, in order to reconcile inflationary prejudices with observations, one has to postulate the existence of cold dark matter that was not directly coupled to the baron-photon plasma in the prerecombination universe (e.g., Blumenthal et al. 1984 and references therein).

Dynamical evolution of CDM in the early universe is now well understood (Peebles 1982; Vittorio & Silk 1985; Bond & Efstathiou 1985). In the CDM model, one assumes that evolution during some early (inflationary) epoch resulted in Gaussian adiabatic density fluctuations with an *initially* scale-invariant power spectrum. Later the evolution of density fluctuations

leads to modification of the power spectrum because of the different growth rates of sub- and superhorizon harmonics during the radiation-dominated era. Thus, in CDM models, the power spectrum of the density field at the epoch of recombination is given by

$$P(k) \propto k^n T^2(k) . \tag{1}$$

The transfer function, $T(k)$, depends mainly on the size of the horizon scale at the matter-radiation equality, $\propto (\Omega h^2)^{-1}$, and is

$$T(k) = \frac{\ln(1 + a_0 k)}{a_0 k} [1 + a_1 k + (a_2 k)^2 + (a_3 k)^3 + (a_4 k)^4]^{-1/4} , \tag{2}$$

where $a_0 = 0.6a_1 = 0.14a_2 = 0.43a_3 = 0.35a_4 = 2.34(\Omega h)^{-1} h^{-1}$ Mpc (Bardeen et al. 1986). On scales greater than the horizon scale at the matter-radiation equality, $\sim 13(\Omega h)^{-1} h^{-1}$ Mpc, the spectrum retains its original form and power slope index $n$. On smaller scales it is modified in a unique, for given $\Omega h$, way. The values of $n$ that are usually considered are $n \simeq 1$, required by the simplest CDM model based on inflation. However, a case has been made also for a tilted CDM model with $n \simeq 0.7$ (Cen et al. 1992).

In models invoking topological defects, such as strings, the evolution of the initial density field can also be calculated, although with significantly more uncertainty because of the possible evolutionary modes of strings when they enter the horizon (Albrecht & Stebbins 1992). In models that involve only baryonic matter, the primeval density fluctuations have to be purely isocurvature, and the evolution of the density field is further complicated by the possible reheating and reionization effects after recombination (e.g., Peebles 1987).

In what follows, we will distinguish between the "primordial spectrum" and what we term the "pregalactic spectrum" of the density field. By "primordial," we will mean the spectrum that was presumably produced during the very early stages of the universe's evolution and which is assumed to be self-similar and characterized only by its power slope index $n$. "Pregalactic," in the terminology of the paper, will refer to the spectrum of the density field after recombination but prior to galaxy formation, e.g., at redshifts greater than 100. In principle, the primordial spectrum can be recovered from the pregalactic one by assuming a transfer function. We will not do this, since it involves various uncertain assumptions, such as the nature of the dark matter, the type of density fluctuations, the values of cosmological parameters, assumptions about the degree and history of reionization after recombination, etc.

In what follows, we will aim to reconstruct the pregalactic density field in the universe from a variety of astronomical data, each data set being responsible for uncovering the spectrum of the density field over a certain range of scales. Because of the theoretical appeal of the CDM models, we will compare the results in each range of scales to the *Ansätze* equations (1) and (2) predicted by inflationary CDM models.

In all models of the early universe evolution, the density field on the largest scales, which were always outside the horizon during the radiation-dominated era, larger than a few hundred $h^{-1}$ Mpc, is expected to have preserved its initial, primordial form. The spectrum of the density distribution on such scales is constrained by the *COBE* DMR data that probe the microwave background anisotropies on angular scales greater than 7°. Assuming a scale-free primordial power spectrum with adiabatic initial conditions, *COBE* DMR data (Smoot et al. 1992; Bennett et al. 1996), after correcting for the Galactic cut, imply a roughly power-law spectrum with $n \simeq 1.1 \pm 0.3$ at the 68% confidence level (Gorski et al. 1996). Normalization to the *COBE* data also fixes the value of the bias parameter $b$ for a given power spectrum of the density field and $\Omega$ (Kashlinsky 1992a; Efstathiou, Bond, & White 1992). CDM models normalized to the *COBE* DMR data require $b > 1$ (e.g., Stompor, Gorski, & Banday 1995).

On smaller scales, the pregalactic density field can be constrained and, as we show below, determined from the astronomical data out to $z$ of a few. In the remainder of this article we recover the pregalactic density field from the various data sets on the present-day universe.

## 3. TWO-POINT GALAXY CORRELATION FUNCTION ON LINEAR SCALES: CONSTRAINING THE SPECTRUM OF LIGHT DISTRIBUTION ON SCALES GREATER THAN 10 $h^{-1}$ Mpc

As was mentioned in § 1, the two-point galaxy correlation function, $\xi(r)$, and the power spectrum represent a pair of three-dimensional Fourier transforms and, for Gaussian density fluctuations, define all properties of the density field. They are related via

$$\xi(r) = \frac{1}{2\pi^2} \int_0^\infty P(k) j_0(kr) k^2 \, dk . \tag{3}$$

Measurements of the two-point correlation function from galaxy catalogs show that on small scales, $\xi(r)$ is very close to a power law $\xi(r) = (r/r_*)^{-1-\gamma}$, where $r_* = 5.5 \, h^{-1}$ Mpc and $\gamma = 0.7$ (Groth & Peebles 1977). This in turn means that the rms fluctuation in galaxy counts over sphere of radius $r$

$$\left\langle \left( \frac{\delta N_{\rm gal}}{N_{\rm gal}} \right)^2 \right\rangle = 3 \int_0^1 \xi(xr) x^2 \, dx = \frac{1}{2\pi^2} \int_0^\infty P(k) W_{\rm TH}(kr) k^2 \, dk \tag{4}$$

is unity on scale $r_8 = [3/(2 - \gamma)]^{-1/(1+\gamma)} r_* \simeq 8 \, h^{-1}$ Mpc (Davis & Peebles 1983). Here $j_n(x)$ is the $n$th-order spherical Bessel function and $W_{\rm TH} = [3j_1(x)/x]^2$. Equation (4) also defines the connection between the "counts-in-cells" analysis used in some galaxy surveys (e.g., Saunders et al. 1991) and the underlying power spectrum or the two-point correlation function, $\xi(r)$.

The data on the correlation function on larger scales are now available from the APM catalog measurements (Maddox et al. 1990, hereafter MESL). The APM survey contains about 2.5 million galaxies in the blue magnitude range $17.5 \leq b_J \leq 20.5$. MESL measured the *projected* two-point angular correlation, $w(\theta)$, down to a systematic error of $w_{\rm pp} \simeq 1.5 \times 10^{-3}$, remaining due to plate-to-plate gradients. These data are consistent with a variety of measurements of $\xi$ from observations at other bands (Picard 1991), catalogs (Collins, Nichol, & Lumdsen 1992) and counts in cells analysis of *IRAS* galaxies (Saunders et al. 1991). These measurements of $w(\theta)$ probe $\xi(r)$ to considerably larger scales than the nonlinear scales of $r < r_8$.

If Galaxy distribution along the line of sight is known, one can relate $w(\theta)$ to the three-dimensional correlation function, $\xi(r)$, via the Limber equation (Limber 1953; Peebles 1980). Its relativistic form is

$$w(\theta) = \int_0^\infty dz \phi(z) \int_{-\infty}^{\infty} d\Delta\xi(r_{12}; z) , \tag{5}$$

where $r_{12}^2 = [\Delta c\, dt/dz]^2 + x^2(z)\theta^2/(1+z)^2$ is the proper length, $x(z)$ is the comoving distance to $z$, $\phi(z) \equiv [(dN/dz)/N_{\rm tot}]^2$ accounts for the fraction of galaxies in the redshift interval $[z; z + dz]$ and $N_{\rm tot} = \int_0^\infty (dN/dz)dz$. The number of galaxies in $dz$ with apparent magnitude $m_l \leq m \leq m_u$ is given by

$$\frac{dN}{dz} = \frac{dV}{dz} \int_{L(m_u)}^{L(m_l)} \Phi(L; z) dL \tag{6}$$

where $dV/dz = cH_0^{-1} x^2(z)/[(1+z)^4(1+\Omega_z)^{1/2}]$ for $\Lambda = 0$, $\Phi(L; z)$ is the galaxy luminosity function at redshift $z$, and $L(m)$ is the absolute luminosity of a galaxy with apparent magnitude $m$ at redshift $z$.

Equation (5) can be rewritten to relate $w(\theta)$ directly to the power spectrum (Kashlinsky 1991*a*; Peacock 1991). Substituting equation (3) in equation (5) and using $\int_{-\infty}^{\infty} j_0[(x^2 + y^2)^{1/2}]dy = \pi J_0(x)$ lead to

$$w(\theta) = \pi \frac{\int_0^\infty dz (c\, dt/dz)^{-1} \phi(z) \int_0^\infty dk\, P(k; z) k J_0(kx\theta/1+z)}{\int_0^\infty P(k; 0) W_{\rm TH}(kr_8) k^2\, dk} , \tag{7}$$

where $J_0(x)$ is the zero-order cylindrical Bessel function. Note that deducing the three-dimensional power spectrum from the projected galaxy angular correlation function is independent of the distortions caused by peculiar velocities in the distribution of galaxies mapped in the redshift space (Kaiser 1987). Throughout the paper we will deal mostly with the shape of the power spectrum rather than its amplitude. Hence, we choose to normalize equation (7) by introducing in the denominator the explicit expression in equation (4) for unity galaxy counts over a sphere of radius $r_8$. As equations (3), (5), and (7) show, a power law for $w(\theta) \propto \theta^{-\gamma}$ implies a power-law behavior for $\xi(r) \propto r^{-1-\gamma}$ or power spectrum $P(k) \propto k^{\gamma-2}$.

The APM survey represents the most accurate and largest data set for determining the correlation function galaxies. On small scales, the projected angular correlation behaves like a power law $w(\theta) \propto \theta^{-\gamma}$ with slope $\gamma = 0.7$. On larger scales, $w(\theta)$ falls off sharply and eventually becomes lost in the systematic errors dominated by the plate-to-plate gradients of the APM catalog, $w_{\rm pp} \simeq 1.5 \times 10^{-3}$. The falloff clearly implies the rollover in $P(k)$ at large scales, or small $k$. The APM catalog contains galaxies down to the limiting blue magnitude of $b_J = 20.5$ corresponding to $z \sim 0.2$. Thus, in order to interpret the data on $w(\theta)$ in terms of the power spectrum today (or at any other coeval epoch), one must eliminate or reduce the possible effects related to evolutionary uncertainties of the luminosities function, $K$-correction, and galaxy clustering.

Various fits have been suggested for the power spectrum to describe the APM data. Kashlinsky (1992*a*, hereafter K92) suggested an empirical fit to the power spetrum to describe the data: On small scales $P(k) \propto k^{\gamma-2}$ to reproduce $w(\theta) \propto \theta^{-\gamma}$ at small angles. On large scales, or $k \leq k_0$, the power spectrum was assumed to go into the Harrison-Zeldovich regime consistent with the *COBE* DMR data. K92 used the APM data divided into six narrow magnitudes of $\Delta m \simeq 0.5$. This way one can reduce the effects of evolution, since such narrow slices are more likely to contain galaxies at similar depths. Approximating the selection function like that of the Lick catalog (Groth & Peebles 1974; Peacock 1991), K92 found that satisfactory fits to the APM data can be obtained for $k_0^{-1} \sim 40\, h^{-1}$ Mpc.

Baugh & Efstathiou (1983, hereafter BE93) have developed an iterative deprojection technique based on the Lucy method (Lucy 1974). They approximated the galaxy selection analytically, and assumed that the time evolution of the power spectrum is scale independent. BE93 then applied the method to invert $w(\theta)$ from the entire APM data set of $17.5 \leq b_J \leq 20.5$. The resultant three-dimensional power spectrum with the error bars from the method uncertainties and the APM data uncertainties is plotted in Figure 7 of BE93. Application of their method to the two-dimensional power spectrum from the entire APM data set led to similar numbers for $P(k)$ (Baugh & Efstathiou 1994).

In terms of CDM models, the APM data require significantly more large-scale power than predicted by the standard CDM model with $\Omega = 1$, $h = 0.5$, $n = 1$ (MESL). Various suggestions have been made to account for the observed excess of large-scale power on scales where the present-day density field is still linear, $r > r_8$. Efstathiou et al. (1990) have noted that the required large-scale power can be reproduced by low-$\Omega$ CDM models, in which case case a nonvanishing cosmological constant would be required to keep the universe flat in accordance with the standard inflationary scenario. Cen et al. (1992) suggested that the excess power can be explained by the so-called tilted CDM model with $n \simeq 0.7$–$0.8$. Either of these modifications, decreasing $\Omega$ or introducing $n < 1$, would boost the large-scale power of the CDM models on scales that are in the linear regime today. (At the same time this would, however, suppress the small-scale power in such models; implications of this are discussed later in this paper).

We now turn to quantifying how good the above fits and models for $P(k)$ are vis à vis the various evolutionary corrections that can effect the accuracy of the various interpretations. The evolution of the luminosity function will affect the selection function of the Limber equation, while evolution of the spectral energy distribution will determine which galaxies appear in

the $B$ band at $z = 0$. Finally, the rate of evolution of the clustering pattern will introduce another redshift-dependent factor in the integrand of the numerator of equation (7). In addition, equation (7) contains a dependence on $\Omega$.

MESL presented their data in two ways: (1) the entire sample of 2.5 million galaxies with $b_J$ magnitudes between 17.5 and 20.5, and (2) the data for subsamples of galaxies binned in six narrow magnitude slices of $\Delta m \simeq 0.5$. In the first data set, which was used in BE93, the galaxies are at very different depths and possibly very different evolutionary stages. The second APM data set used in K92 is more immune from effects of evolution, since it is more likely to separate galaxies at different depths, and any evolution can be more readily uncovered and corrected for. We thus consider the APM data on $w(\theta)$ for the six slices each $\Delta m \simeq 0.5$ in width.

Figure 1 plots the selection function, $z\phi(z)$, for the six slices with $\Delta m \simeq 0.5$ of the APM survey from $b_J = 17.5$ to $b_J = 20.5$. The luminosity function in equation (6) was adopted from Loveday et al. (1992), i.e., the Schechter (1976) luminosity function with $M^*_{b_J} = -19.5$ for $h = 1$ and $\alpha = -1$. The relativistic $K$-correction was modeled as $\delta m = Kz$ with $K = 3$, which adequately describes galactic spectra in the visible bands (cf. Yoshii & Takahara 1988). Solid lines correspond to $\Omega = 0.1$, and dotted lines to $\Omega = 1$, and no evolution was assumed. One can see that there is little dependence on $\Omega$. Similarly, there would be little change for other plausible values of $0 \leq K \leq 4$. The nearest slice of the APM galaxies contains galaxies typically lying at $z \simeq 0.07$, and the farthest slice contains galaxies at $z \simeq 0.2$, so a certain amount of evolution could have occurred. There is no overlap at the FWHM level between galaxies in the nearest and most remote slices, although a certain overlap exists between galaxies in the nearby slices.

On comoving scales less than $r_8$, the present-day density fluctuations are nonlinear, and the clustering pattern has been strongly distorted by gravitational evolution (e.g., Davis et al. 1985). On larger scales, the density field is still in the linear regime and the clustering pattern there is likely to have preserved the original power spectrum of the density field. We use the small scales, $r \ll r_8$, where the power spectrum is well known and its evolution with $z$ better understood, to constrain the possible evolutionary effects that can plague the APM data interpretation.

As $\theta \to 0$, the APM two-point correlation function is approximated well by a pure power law. At the same time, for small angular separations, the contribution to equation (5) from $\xi(r)$ at large separations becomes negligibly small. Thus, in the limit of small angular separations, the three-dimensional two-point correlation function at $z = 0$ can be taken from the Lick catalog to be $\xi(r) = (r/r_*)^{-1-\gamma}$ with $r_* = 5.5\ h^{-1}$ Mpc. The time dependence of $\xi(r)$ can be modeled in the very nonlinear regime as $\xi(r; z) = \xi(r; 0)\Psi^2(z)$. Two extremes of clustering evolution are generally considered for very small scales (Peebles 1980): when clustering is stable in comoving coordinates $\Psi^2(z) = (1 + z)^{-3}$, and when it is stable in proper coordinates $\Psi^2(z) = (1 + z)^{-1-\gamma}$. Thus, for small scales, the evolutionary effects must be constrained to match the APM data for all six slices: $w(\theta) = A_{w,\mathrm{slice}}\,\theta^{-\gamma}$. Substituting $\xi(r; z) = (r/r_*)^{-1-\gamma}\Psi^2(z)$ into equation (5) leads to

$$A_w = \frac{\Gamma(1/2)\Gamma(\gamma/2)}{\Gamma[(1+\gamma)/2]}\left(\frac{r_*}{cH_0^{-1}}\right)^{1+\gamma}\int_0^\infty \phi(z)\left[\frac{cH_0^{-1}(1+z)}{x(z)}\right]^{\gamma}\Psi^2(z)(1+z)^2\sqrt{1+\Omega z}\,dz\ . \tag{8}$$

Comparison between equation (8) and the amplitude measured in the APM data provides an integral constraint on the amount of possible evolution.

Figure 2 plots the data from the APM survey (MESL) divided into six narrow magnitude bins. The magnitude limits for each bin are shown on the top of each panel. The data are plotted with open triangles. The power-law fits corresponding to $A_w\,\theta^{-\gamma}$ are plotted with two sets of straight lines. Dashed lines are for $\Omega = 1$, and dotted lines are for $\Omega = 0.1$ and $\Lambda = 0$. The two lines of each type correspond to a clustering pattern stable in comoving (*lower lines*) and proper coordinates. The amplitudes $A_w$ are shown for $K = 3$. One can see that no-evolution models describe the low-angle behavior of $w(\theta)$ extremely well. The dependence on $\Omega$ can be neglected, and the dependence on the precise rate of the evolution of clustering pattern is also small. For clarity of the figure, we do not show the lines for other values of $K$, but note that the change is very small. Increasing the value of $K$ would move the lines a little higher, and decreasing it to less than 3 would make them lie exactly on

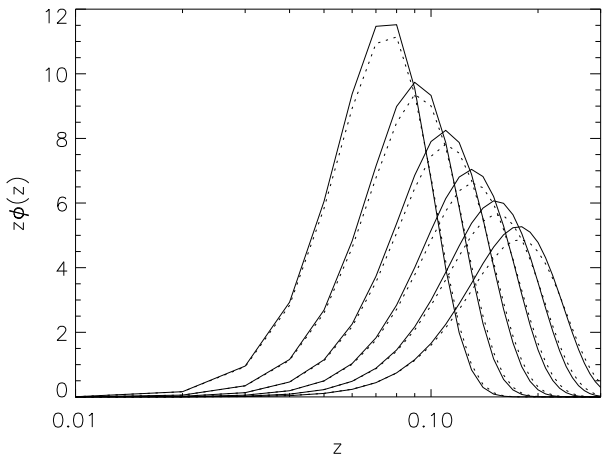


FIG. 1.—Selection function for the six 0.5 mag wide slices of the APM data. The lines are computed using the $K$-correction as $\delta m = Kz$ with $K = 3$, but the dependence on $K$ is weak for $K \leq 4$. Solid lines correspond to $\Omega = 0.1$ and dotted lines to $\Omega = 1$. The six curves of each type correspond to the magnitude range of each of the APM slices shown on top of the boxes in Fig. 2.

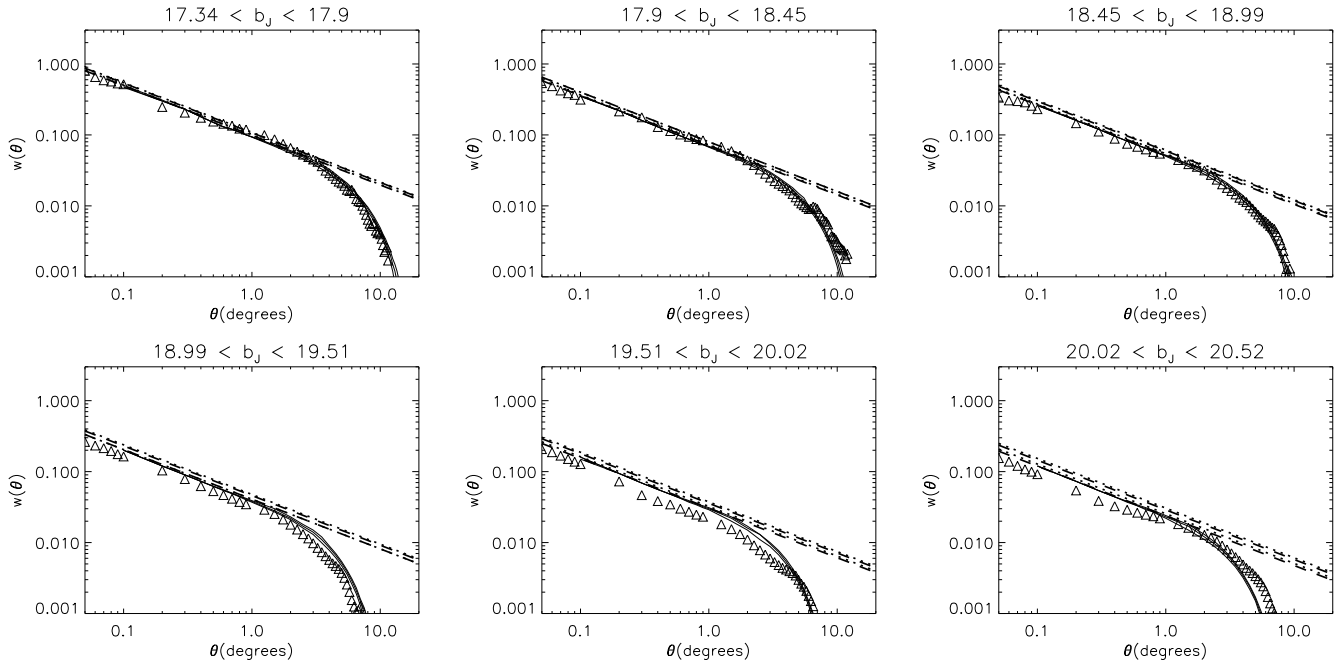


FIG. 2.—Open triangles show the APM data in the narrow magnitude slices. The magnitude ranges are shown on top of the boxes. Thick dashed lines are for $\Omega = 1$ and a power law $\xi(r)$, which should give a good fit to the data at small angular scales. Thick dotted lines, that mostly merge with the thick dashed lines, show the power-law fit for $\Omega = 0.1$. The upper thick lines of each type are for the clustering pattern stable in physical coordinates, i.e., $\xi(r; z) = (r/r_*)^{-1.7}(1 + z)^{-1.7}$. Lower thick lines correspond to a clustering pattern that is stable in comoving coordinates: $\xi(r; z) = (r/r_*)^{-1.7}(1 + z)^{-3}$. Three solid lines correspond to the best BE93 fit to the APM power spectrum and $\pm 1$ standard deviation uncertainty. For the BE93 lines the power spectrum was taken to evolve $\propto(1 + z)^{-3}$. The numbers are shown for $K = 3$.

top of the data at small angular scales. Similarly, making the clustering pattern evolve a little faster than $\Psi^2(z) = (1 + z)^{-3}$, as is suggested by simulations of nonlinear gravitational clustering (Melott 1992), would shift the lines even closer to the data points. Thus, we conclude that the APM data are consistent with little or no evolution out to the epochs accessible to the APM magnitude limit of $b_J = 20.5$. The slight excess in the computed amplitude $A_w$ can be easily reduced by zero by adopting a slightly lower value of $K$ or requiring the clustering pattern to evolve faster than $\Psi^2(z) = (1 + z)^{-3}$. The first of these is quite reasonable given the evolution of stellar populations in the relevant bands (e.g., Bruzual 1983). The second could be required if mergers play a significant role in the evolution of clustering on nonlinear scales (Melott 1992); this may even be suggested by the deep galaxy counts data (Broadhurst, Ellis, & Glazebrook 1992). Thus, we conclude that luminosity evolution plays a minor role out to $z \simeq 0.2$ for the standard population of blue galaxies with $b_J \leq 20.5$. The no-evolution models with nonlinear clustering, stable in comoving coordinates, can be used sufficiently accurately in interpretating the APM data on $w(\theta)$ in terms of the underlying power spectrum of galaxy distribution.

Thin solid lines in Figure 2 show the BE93 fits to the six slices of the APM data, assuming no luminosity evolution and with the luminosity function adopted from Loveday et al. (1992). The three lines correspond to the best determined $P(k)$ of BE93 and to 1 standard deviation uncertainty. The clustering pattern was assumed to be stable in comoving coordinates on all scales. The BE93 power spectrum fits the data well at the various depths. It underpredicts the power on large scales by a small margin for the most distant of the APM slices. This, however, can be accounted for by assuming that the power spectrum on linear scales evolves less rapidly with redshift than the $\Psi^2(z) = (1 + z)^{-3}$ adopted from the nonlinear scales. Indeed, linear scales should evolve differently in accordance with the growth predictions in the linear regime. In principle, one can try to reproduce the consistent evolution of the power spectrum on all scales following the prescription of Hamilton et al. (1991). However, it is not yet clear how well such fits work for arbitrary cosmologies and (non–power-law) power spectra (cf. Peacock & Dodds 1994). The fit of the BE93 power spectrum to the APM data is good, and we adopt it as a reasonable approximation to the power spectrum of galaxy distribution. The K92 fit is essentially the same as shown in Figure 1 of the K92 paper, and for brevity and clarity we do not show this set of lines in Figure 2, other than to point out that the BE93 power spectrum fits the APM data much better than the earlier K92 empirical fit.

The K92 and BE93 power spectra fit the clustering hierarchy today over both linear and nonlinear scales. On linear scales the power spectrum today should reflect initial conditions, but on scales less than $r_8$ the initial power spectrum was distorted by gravitational effects. CDM models predict a power spectrum only in the linear regime, so it makes little sense to plot them in the already condensed Figure 2. In order to constrain CDM models from the binned APM data, we proceed as follows: The APM data are accurate for $w(\theta) > w_{pp} \simeq 1.5 \times 10^{-3}$, and the small angular scales analysis suggested that evolutionary effects are small for scales and depths probed by the APM survey. The largest angular scales, where $w(\theta)$ can still be probed, are dominated by contributions from linear scales, $r > r_8$, and the data should be reproduced by equations (1) and (2) within the framework of CDM models.

Thus, for a given CDM model specified by $n$ and $\Omega h$, we computed the angular scale, $\theta(w)$, on which the predicted angular correlation function drops to the value $w$. Figure 3 plots the resultant $\theta(w)$ versus the mean magnitude, $b_J$, of the slices in

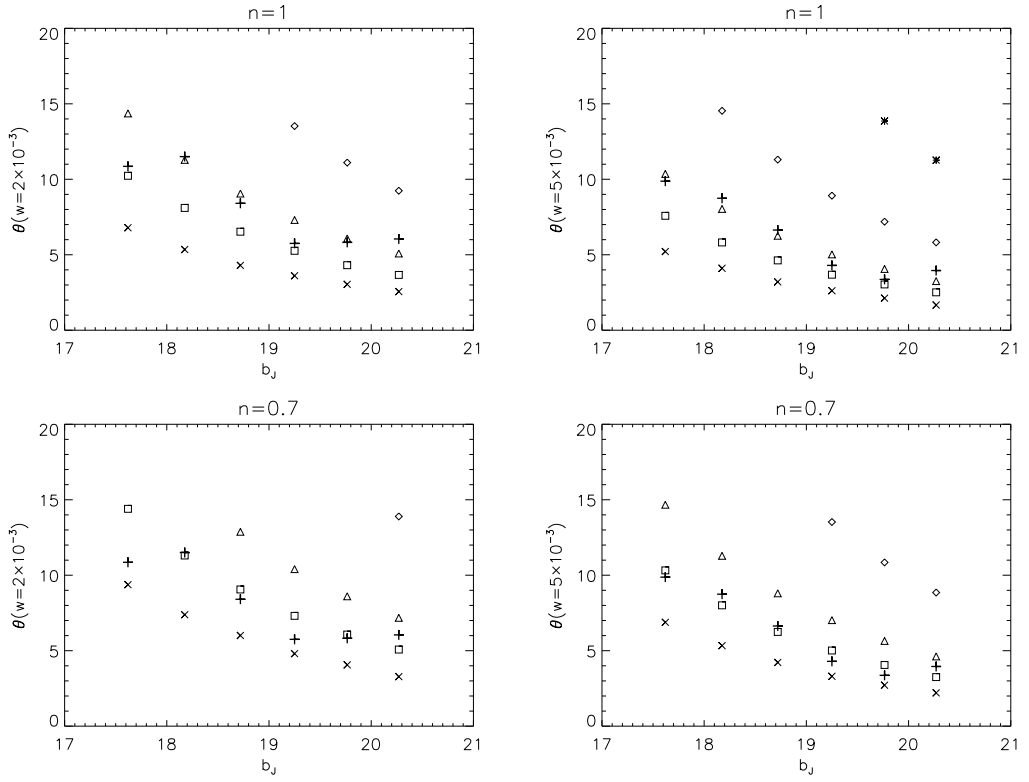


FIG. 3.—Angular scale, $\theta(w)$, at which the projected angular correlation reaches a given value, $w$, plotted against the mean blue magnitude of the APM six slices. Left-hand panels correspond to $w = 2 \times 10^{-3}$, which is just above the systematic error, $w_{pp} \simeq 1.5 \times 10^{-3}$. Right-hand panels are for $w = 5 \times 10^{-3}$. Thick plus signs correspond to the APM data plotted in Fig. 2. The data are compared with CDM predictions: upper panels show the values of $\theta(w)$ for $n = 1$ and lower panels for the tilted CDM model with $n = 0.7$. Crosses correspond to $\Omega h = 0.5$, open squares to $\Omega h = 0.3$, triangles to $\Omega h = 0.2$, diamonds to $\Omega h = 0.1$, and asterisks to $\Omega h = 0.05$. Only CDM models that match the observed values (*plus signs*) would be consistent with APM data.

Figure 2 for the APM data and for predictions of the standard ($n = 1$; *upper panels*) and tilted ($n = 0.7$; *lower panels*) CDM models. The left-hand panels are for $w = 2 \times 10^{-3}$, which is just above the systematic error of $w_{pp} = 1.5 \times 10^{-3}$ induced by the plate-to-plate gradients in the APM survey. The right-hand panels are for $w = 5 \times 10^{-3}$, which is significantly larger than $w_{pp}$ and should be quite accurate. The thick plus signs show the values of $\theta(w)$ derived from the APM data. CDM models are shown with the other signs: crosses correspond to $\Omega h = 0.5$, squares to $\Omega h = 0.3$, triangles to $\Omega h = 0.2$, diamonds by $\Omega h = 0.1$, and asterisks to $\Omega h = 0.05$.

As was mentioned, the values of $\theta(w = 5 \times 10^{-3})$ are more reliable, but there is general agreement between the CDM fits and angular scales at both values of $w$. There is also consistency between the fits for various slices or depths. The fits in Figure 3 show that the linear part of the APM data can be described by CDM models, which would then require $\Omega h = 0.2$ if $n = 1$ or $\Omega h = 0.3$ if $n = 0.7$. Increasing $n$ above 0.7 would require even lower values of $\Omega h$. The limit on $\Omega h$ required by CDM models for $n = 1$ is in good agreement with what was claimed before Efstathiou et al. (1990). It is worth noting that the limits on the power parameter $\Omega h$ for the CDM models come from the nearby slices. The differences in the values of $\theta(w = 5 \times 10^{-3})$ between CDM models of different $\Omega h$ are most profound for the slices that are nearest (and least affected by any evolution). For the first three slices the APM data (*plus signs*) would overlap with CDM predictions only for $\Omega h = 0.2$ if $n = 1$ and for $\Omega h = 0.3$ if $n = 0.7$; CDM models with both smaller and larger $\Omega h$ would predict values of the angular scale $\theta(w)$, where $w = 5 \times 10^{-3} \simeq 3.3 w_{pp}$, different from what is observed. The limit on $\Omega h$ ($= 0.3$) for the tilted model is significantly lower than what was suggested before in Cen et al. (1992), who used all the APM galaxies lumped together and then scaled to the depth of the Lick catalog. Thus, even if the primordial $n$ were as low as 0.7, one would still require low $\Omega$ to fit the APM data with the CDM power spectrum.

Strictly speaking, the above discussion applies only to the distribution of light (galaxies). In order to relate the power spectrum of galaxy distribution to that of mass, one has to make assumptions about biasing or whether and how the light traces mass. The most economical and commonly made assumption is that of linear biasing (Kaiser 1984), i.e., that light traces mass at least to within a scale-independent constant. We followed this assumption in this section, but it must be remembered that the plots in Figures 2 and 3 refer only to the distribution of luminous matter. The next section discusses this assumption in more detail, and there we propose an empirical justification for it based on comparing the density field of the APM survey to that probed by the velocity data.

Assuming that light indeed traces mass, information on the initial (pregalactic) power spectrum in present-day galaxy catalogs is preserved only on scales where the density field is still in the linear regime, $r > r_8$. Thus Figure 4 plots the rms density fluctuation $\Delta(M)$ over a sphere containing mass $M$ versus the comoving scale this mass subtends for the spectra required by the APM data. It is plotted in units of $\Delta_8$, the rms fluctuation over a sphere of radius $r_8$, and the numbers are shown for $r > 10\ h^{-1}$ Mpc where the galaxy density field is still in the linear regime. This ratio is used because in the linear

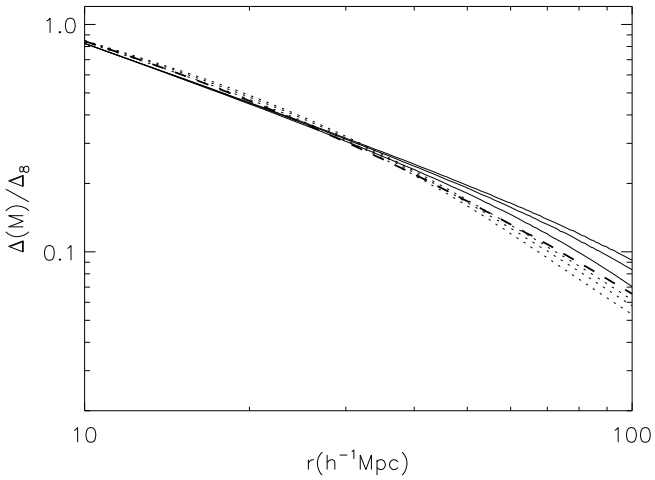


FIG. 4.—Values of the rms density contrast, $\Delta(M)$, in units of $\Delta_8$, plotted for the various fits to the APM data. Dotted lines show the BE93 fit with 1 standard deviation uncertainty. Solid lines correspond to the K92 fit with $k_0 = 35, 40, 50\ h^{-1}$ Mpc from the bottom up. The thick dashed line corresponds to CDM models with $\Omega h = 0.2, n = 1$ and $\Omega h = 0.3, n = 0.7$.

regime it is roughly epoch independent, and also because for linear biasing, the quantity $\Delta(M)/\Delta_8$ recovered from the APM data is independent of the (constant) biasing factor $b$. Solid lines are the K92 power spectra with the transition scale $k_0^{-1} = 35$, 45, 55 $h^{-1}$ Mpc from the bottom up. Dashed lines correspond to the BE93 power spectrum with three lines showing the mean and $\pm 1$ standard deviation uncertainty. The CDM models that fit the APM data in six narrow magnitude slices are shown with thick dashed lines: $n = 1$, $\Omega h = 0.2$ and $n = 0.7$, $\Omega h = 0.3$. (The two models would essentially overlap over the range of scales plotted in Figure 4). The various fits to the data practically overlap on scales less than 50 $h^{-1}$ Mpc. On larger scales the BE93 spectrum, which fits the APM data best, gives the least amount of large-scale power. Within the uncertainty of the methods, the CDM models required by the APM data reproduce roughly the same $\Delta(M)/\Delta_8$ ratio as the BE93 spectrum on scales less than 100 $h^{-1}$ Mpc.

*The quantity $\Delta(M)/\Delta_8$ plotted in Figure 4 is independent of the bias factor provided that the latter is scale independent. It also measures the spectrum of the density field in linear regime and is approximately independent of the redshift at which it is evaluated. These are the main reasons why we choose to reconstruct this quantity from various data sets in this paper.*

To conclude this section:

1. By analyzing APM Catalog data in narrow magnitude slices, it was demonstrated that evolutionary effects are unlikely to affect interpretation of the APM data.
2. The power spectrum derived by BE93 provides a good fit to the APM data at all depths.
3. Assuming that light traces mass, the APM data can be fitted at all depths by the standard CDM models with $n = 1$ if $\Omega h \simeq 0.2$.
4. Tilted CDM models will require $\Omega h \simeq 0.3$ if $n = 0.7$ and lower values if $n$ is increased.
5. In any case, all the above fits give practically identical numbers for $\Delta(M)/\Delta_8$ on linear scales below 50 $h^{-1}$ Mpc. This quantity measures density field in the linear regime and is approximately redshift independent. If the possible bias factor is scale independent, the quantity $\Delta(M)/\Delta_8$ determined from the APM data is independent of the bias factor.
6. Figure 4 demonstrates the consistency of this approach, and we conclude that, provided that light traces mass, the pregalactic density field on these scales is close to that drawn in the figure.

## 4. PECULIAR VELOCITY FIELD VERSUS GALAXY CORRELATION DATA: CONSTRAINING Ω AND THE BIAS FACTOR

The previous section established the spectrum of galaxy distribution on scales 10 $h^{-1}$ Mpc $< r <$ (60–100) $h^{-1}$ Mpc. In order to reliably identify it with the spectrum of the pregalactic density field, one has to establish the relation between the light and mass distributions. Furthermore, as was discussed in the framework of the CDM models, APM data would require a low-Ω universe. An independent test of these findings and assumptions can be provided by intercomparison between the observed properties of peculiar velocity and density fields (Kashlinsky 1992*b*, 1994). We address these questions in this section.

Measurements of peculiar velocities provide one with a direct probe of the mass distribution in the universe, and thus set strong limits on the large-scale structure models (e.g., Vittorio, Juszkiewicz, & Davis 1987). Recent advances wih the new distance indicators (Djorgovski & Davis 1987; Dressler et al. 1987*a*) allowed one to measure the peculiar flows in the local part of the universe up to $\sim$50–100 $h^{-1}$ Mpc (see Strauss & Willick 1995 for a review). The results from using the fundamental-plane properties of elliptical galaxies (Dressler et al. 1987*b*) suggest a large coherence length and amplitude of the local peculiar velocity field. The results from analysis of 1355 spirals using the Tully-Fisher relation to determine distances (Mathewson, Ford, & Buchorn 1992) would lead to an even larger coherence length and a similar amplitude. Other samples are also in agreement with the Great Attractor findings (e.g., Willick 1990). In a more controversial finding, Postman & Lauer (1995) found from analysis of clusters of galaxies that the peculiar flows can be coherent over a much larger scale than the Great Atractor findings. All the results indicate significant deviations from the Hubble flow with a large coherence length.

Since peculiar velocities probe the mass distribution and also depend on the density parameter $\Omega$, one can determine the latter by comparing the mass distribution implied by the velocity field with the observed distribution of galaxies. The density parameter is thus determined to within the uncertainty of the bias factor $b$ by determining the factor $\Omega^{0.6}/b$. There are various ways to use this information to get at $\Omega$. Bertschinger & Dekel (1989) developed the POTENT method, whereby the mass distribution is reconstructed by using the analog of the Bernoulli equation for irrotational flows. They used the method to analyze in great detail and accuracy the peculiar velocity field out to about 60 $h^{-1}$ Mpc (Bertschinger et al. 1990). In Dekel et al. (1993), they compared the previously determined velocity field with the observed distribution of galaxies, and concluded that the best fit is achieved with $\Omega^{0.6}/b \simeq 1$.

A different method was presented by Kashlinsky (1992*b*) and was based on comparing the velocity correlation function with the galaxy correlation function from the APM catalog; this led to low values of $\Omega^{0.6}/b \simeq 0.2$–$0.3$. We present below a more detailed analysis based on the latter scheme, and show that the results are indeed suggestive of low values of the density parameter. We also show that the results are in agreement with the scale-independent bias factor.

We define the dot velocity correlation function $v(r) = \langle \boldsymbol{v}(\boldsymbol{x} + \boldsymbol{r}) \cdot \boldsymbol{v}(\boldsymbol{x}) \rangle$ (Vittorio et al. 1987; Peebles 1987)

$$v(r) = \frac{1}{2\pi^2} \int_0^\infty |v_k|^2 j_0(kr) k^2 \, dk \ . \tag{9}$$

Since gravity force is conservative, the flow caused by it must be irrotational. For irrotational flow the $k$th component of the Fourier transform of the peculiar velocity field is $\boldsymbol{v}_k = -i\boldsymbol{k} H_0 f(\Omega) \delta_k / k^2$, where $f(\Omega) = \partial \ln \delta_k / \partial \ln t$. For the case of zero cosmological constant $f(\Omega) = \Omega^{0.6}/b$. If the cosmological constant, $\Lambda$, is not zero, $f(\Omega)$ will be different, but for the most interesting case of $\Omega + \Lambda/3H_0^2 = 1$, the above approximation would work very well (Lahav et al. 1991). Equations (3), (9), and (10) are also valid for the filtered fields in which case both $v(r)$ and $\xi(r)$ must be replaced with their filtered versions.

Assuming that light traces mass to within a constant bias factor, $b$, substituting $v_k$ into equation (9), and then taking the Laplacian operator of both sides, would lead to

$$\nabla^2 v(r) = -\frac{\Omega^{1.2}}{b^2} H_0^2 \, \xi(r) \tag{10}$$

where it was used $\nabla^2 j_0(kr) = -k^2 j_0(kr)$ along with equation (3). This equation was evaluated independently in Kashlinsky (1992*b*) and Juszkiewicz & Yahil (1989) and it can be used to relate the *data* on both peculiar velocity field and galaxy correlation function to get $\Omega^{0.6}/b$ (Kashlinsky 1992*b*, 1994). The advantage of using equation (10) rather than the power spectrum data in conjunction with equation (9) (e.g., Kaiser 1983) is that equation (10) can be integrated to contain only the scales over which the *data* on both $\xi(r)$ and $v(r)$ are known, while in the former case assumptions have to be made about the power spectrum over the wavelengths inaccessible to observations (Vittorio et al. 1987). (Of course, the data $\xi(r)$ are in effect on integral constraint on $P(k)$ over the infinite range of wavelengths). Equation (10) can be solved to give the velocity correlation function in terms of $\xi(r)$:

$$v(r) = v(0) - \frac{\Omega^{1.2}}{b^2} H_0^2 \left[ J_2(r) - \frac{J_3(r)}{r} \right], \tag{11}$$

where it is defined $J_n(r) \equiv \int_0^r \xi(x) x^{n-1} \, dx$. Only one of the constants of integration remains in equation (11). The other constant of integration vanishes because the velocity field must be finite at $r = 0$. The constant of integration remaining in equation (11) is just the "central" velocity dispersion, $v(0) = \langle v^2 \rangle$.

Strictly speaking, in order to use equation (10), the data on both $v(r)$ and $\xi(r)$ must come from the same region of the universe. Since the current velocity data sample galaxies within a radius of $\sim 100$ $h^{-1}$ Mpc, the numbers for $\xi(r)$ must come from the "local" surveys such as the CfA survey (Geller & Huchra 1989). The CfA redshift survey is complete out to $m_B \leq 15.5$, and for the relevant scales, $r \simeq 40$ $h^{-1}$ Mpc, the correlation function in the CfA survey essentially coincides with the one determined from the APM catalog (Da Costa et al. 1994; Vogeley et al. 1992). In fact, the numbers in this section are in good agreement with each other when evaluated for $\xi(r)$ taken from the CfA survey, the power-law model, or the BE93 or K92 fits to the APM data on $w(\theta)$. The galaxy correlation function on the relevant scales taken from the APM data, as discussed in the previous section, is plotted in Figure 11; for the CfA survey $\xi(r)$ is plotted in Figure 3 of Vogeley et al. (1992).

The observed correlation function of galaxies would predict large velocities if $\Omega^{0.6}/b = 1$. For the power law $\xi(r) = (r/r_*)^{-1-\gamma}$, equation (11) would lead to

$$[v(0) - v(r)]^{1/2} = \frac{H_0 r_*}{[(1-\gamma)(2-\gamma)]^{1/2}} \left( \frac{\Omega^{0.6}}{b} \right) \left( \frac{r}{r_*} \right)^{(1-\gamma)/2} = 881 \left( \frac{\Omega^{0.6}}{b} \right) \left( \frac{r}{r_*} \right)^{0.15} \text{ km s}^{-1} \ .$$

for $\gamma = 0.7$. The value of $[v(0) - v(r)]^{1/2}$ for $\Omega^{0.6}/b = 1$ would be significantly larger than the data on peculiar velocities at 40 or 60 $h^{-1}$ Mpc of Bertschinger et al. (1990) (see Table 1). Figure 5 plots the predicted value of $[v(0) - v(r)]^{1/2}$ computed according to equation (11) for $\Omega^{0.6}/b = 1$; the numbers in Figure 5 scale as $\Omega^{0.6}/b$. The data on $\xi(r)$ from which the lines in Figure 5 were computed are for the APM correlation function using the BE93 deprojection (*solid lines*) and the correlation function of the CfA survey from Vogeley et al. (1992) (*dashed line*). The three solid lines correspond to 1 standard deviation uncertainty in BE93. CfA survey measures $\xi(r)$ out to only $\simeq 40$ $h^{-1}$ Mpc; hence the line ends there. The lines show that there is good agreement with the dot velocity correlation function values computed "locally" (CfA) and "globally" (APM). There is also good agreement between the shape of the bulk velocity flows in the Great Attractor region (Bertschinger et al. 1990) and Figure 5. This is consistent with the assumption of a scale-independent bias parameter $b$.

TABLE 1

DATA FROM BERTSCHINGER et al. 1990

| Parameter | $r = 0$ | $r = 40\ h^{-1}$ Mpc | $r = 60\ h^{-1}$ Mpc |
|---|---|---|---|
| $V(r)$ (km s$^{-1}$)..... | $457 \pm 61$ | $388 \pm 67$ | $327 \pm 82$ |
| $(L, B)$..... | $(156 \pm 7, -19 \pm 12)$ | $(177 \pm 9, -15 \pm 17)$ | $(194 \pm 13, 5 \pm 26)$ |

We now ask the following question: given the *measurement* of $v(r)$ on some scale, what should one expect to find for $v(0)$ given the *data* on $\xi(r)$? This can be evaluated from

$$v(0) = v(r) + \frac{\Omega^{1.2}}{b^2} H_0^2 \left[ J_2(r) - \frac{J_3(r)}{r} \right]. \tag{12}$$

In order to evaluate $v(0)$ from $v(r)$, we use the numbers from the POTENT analysis (Bertschinger et al. 1990) that computed the bulk velocity $V(r)$ field after filtering the data with a Gaussian filter of filtering length $r_f = 12\ h^{-1}$ Mpc. The numbers from their analysis of the velocity field are given in Table 1, which shows the values of $V(r)$, the amplitude and direction, for three different values of $r$.

The data with which $v(0)$ ought to be compared are admittedly incomplete, but it is generally thought that for a non-filtered velocity field, $[v(0)]^{1/2} \sim 500$–$600$ km s$^{-1}$ (cf. Peebles 1987). This also follows from the numbers for velocity dispersions in typical collapsed systems, such as groups of galaxies. Local measure of $[v(0)]^{1/2}$ is probably the dipole velocity which is observed to be 630 km s$^{-1}$ with a very small error. (The direction of the microwave background dipole roughly coincides with the velocity vector from Bertschinger et al. 1990 in Table 1.) Since $v(r) \to 0$ as $r \to \infty$, equation (12) shows that the linear perturbative expression for $v(0)$ is proportional to $J_2(r \to \infty) \equiv J_{2,\infty}$. In this case, because $\xi(r) \propto r^{-1.7}$ at small scales, a nonnegligible contribution to $v(0)$ comes from nonlinear scales. This suggests the importance of smoothing when evaluating $v(0)$ directly from the data. Peebles (1988) utilized the exact (nonperturbative) Layzer-Irvine cosmic energy equation to compute $v(0)$ using the value of $J_{2,\infty} = 164e^{\pm 0.15}\ h^{-2}$ Mpc$^2$ evaluated from the Lick data (Clutton-Brock & Peebles 1981). He obtained $[v(0)]^{1/2} \simeq 500$–$600$ km s$^{-1}$ for $\Omega$ in the range 0.2–0.3, in reasonable agreement with this discussion. For comparison, integrating over $\xi(r)$, evaluated from the BE93 deprojection of the APM data, gives $J_{2,\infty} \simeq 170 \pm 5\ h^{-2}$ Mpc$^2$, while for the CfA data from Vogeley et al. (1992), one obtains $J_{2,\infty} \simeq 186\ h^{-2}$ Mpc$^2$. Both are in agreement with the numbers used in Peebles's (1988) analysis.

Table 2 shows the values of $[v(0)]^{1/2}$ evaluated from equation (12), given the velocity data input on $v(r) \simeq V^2(r)$ at $r = 40$ and $60\ h^{-1}$ Mpc from Bertschinger et al. (1990). The columns show numbers for $\xi(r)$ on scales $\leq 60\ h^{-1}$ Mpc computed according to pure power law, $\xi(r) = (r/r_*)^{-1-\gamma}$; the K92 and BE93 fits to the APM data; and the CfA data on $\xi(r)$ from Vogeley et al. (1992) at $r < 40\ h^{-1}$ Mpc. The first column gives the filtering radius in $h^{-1}$ Mpc, the second gives the value of $\Omega^{0.6}/b$ used in equation (3), and the next seven columns give the values of $[v(0)]^{1/2}$ in km s$^{-1}$ computed according to equation (12) for the various $\xi(r)$. The first four rows show the numbers with no filtering; the last four rows show the numbers for $r_f = 12\ h^{-1}$ Mpc used in the analysis of the velocity field Bertschinger et al. (1990). The data for the CfA measured $\xi(r)$ are shown only for $r = 40\ h^{-1}$ Mpc, the scale to which the CfA data can probe $\xi(r)$. We have not shown the filtered values for the CfA $\xi(r)$ because the latter was not measured out to large enough scales to make filtering with $r_f = 12\ h^{-1}$ Mpc meaningful.

The various fits to the galaxy correlation function give similar numbers, which shows the robustness of the various fitting methods. The numbers for $v(0)$ in Table 2 are also in good agreement with the asymptotic value of $v(0) = (\Omega^{1.2}/b^2)H_0^2 J_{2,\infty}$ discussed earlier; e.g., for the values of $J_{2,\infty}$ computed earlier for the CfA and APM data, one gets $[v(0)]^{1/2} \simeq 1364$ and 1304 km s$^{-1}$, respectively. The data on $\xi(r)$ determined from the CfA survey come from the region that includes galaxies used in the peculiar velocity analyses (Faber et al. 1989), and agrees well with the values of $v(0)$ predicted by the APM data. This in turn

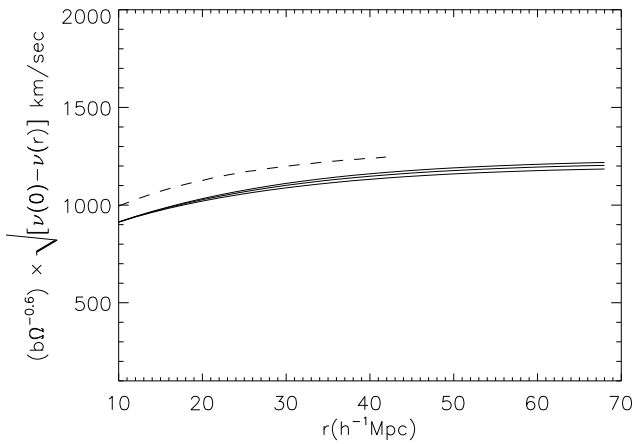


FIG. 5.—Values of the "typical velocity" profile derived from eq. (11) using the data on the galaxy correlation function, $\xi(r)$, plotted for $\Omega^{0.6}/b = 1$. The dashed line corresponds to the velocity field from the CfA data on $\xi(r)$, and solid lines correspond to $\xi(r)$ given by the BE93 fit to the APM data with 1 standard deviation uncertainty.

TABLE 2

$[v(0)]^{1/2}$ (km s$^{-1}$) COMPUTED ACCORDING TO EQUATION (12) FOR VARIOUS FITS TO $\xi(r)$

| $r_f$ | $\Omega^{0.6}/b$ | Power law $\xi(r) = (r/r_*)^{-1.7}$ 40 Mpc $h^{-1}$ | K92 60 Mpc $h^{-1}$ | K92 40 Mpc $h^{-1}$ | BE93 60 Mpc $h^{-1}$ | BE93 40 Mpc $h^{-1}$ | CfA 60 Mpc $h^{-1}$ | CfA 40 Mpc $h^{-1}$ |
|---|---|---|---|---|---|---|---|---|
| 0..... | 1.00 | 1184 | 1230 | 1180 | 1220 | 1212 | 1239 | 1230 |
| 0..... | 0.50 | 678 | 681 | 674 | 669 | 682 | 693 | 732 |
| 0..... | 0.33 | 538 | 515 | 537 | 512 | 545 | 517 | 567 |
| 0..... | 0.25 | 478 | 443 | 478 | 442 | 483 | 445 | 497 |
| 12..... | 1.00 | 613 | 691 | 604 | 673 | 608 | 657 | ... |
| 12..... | 0.50 | 455 | 449 | 452 | 442 | 453 | 435 | ... |
| 12..... | 0.33 | 419 | 387 | 418 | 384 | 418 | 380 | ... |
| 12..... | 0.25 | 406 | 363 | 405 | 361 | 405 | 359 | ... |

means that the Great Attractor is a typical, rather than rare, mass concentration in the universe. There is very good agreement between the numbers in Table 2 evaluated at both 40 and 60 $h^{-1}$ Mpc. This is consistent with the constant bias factor over at least this range of scales.

Low values of $\Omega$ are implied by this analysis. For example, the nonfiltered field, the predicted value of $[v(0)]^{1/2}$ should be compared with the data on the dipole velocity of only 600 km s$^{-1}$. Also, if $\Omega^{0.6}/b$ were as high as unity, the typical velocity dispersion in the collapsed systems would be around 1300 km s$^{-1}$, corresponding to X-ray temperatures greater than 10 keV. Observations, however, suggest that typical collapsed structures, such as groups and poor clusters of galaxies, have velocity dispersion $\simeq 500$ km s$^{-1}$, and rich X-ray–emitting clusters contain only a small fraction of all galaxies. For the filtered field with $r_f = 12\,h^{-1}$ Mpc, the predictions should be compared wth the value from the Bertschinger et al. (1990) analysis that gives $457 \pm 61$ km s$^{-1}$. Again the best agreement between the data and $v(0)$ would be achieved for $\Omega^{0.6}/b \simeq 0.2$–0.3. The fact that we reach essentially the same conclusions when comparing the filtered $v(r)$ is reassuring.

Thus, the above analysis suggests that low-$\Omega$ universe may not be in conflict with the data on peculiar velocities and may in fact be even suggested by the latter. Similar conclusions are reached applying the least-action method (Peebles 1989, 1990) to the dynamics of the Local Group (Shaya et al. 1995). We have not quantified the conclusions from Table 2 in statistical terms and, hence, take them only as suggestive. Below we propose a further extension of this discussion that may determine the values of $\Omega^{0.6}/b$ in the new data sets on peculiar flows.

A similar analysis can be applied to the components of the velocity tensor:

$$U_{ij} = \langle \boldsymbol{v}_i(\boldsymbol{x} + \boldsymbol{r}) \cdot \boldsymbol{v}_j(\boldsymbol{x}) \rangle \equiv \Sigma(r)\delta_{ij} + [\Pi(r) - \Sigma(r)] \frac{\boldsymbol{r}_i \cdot \boldsymbol{r}_j}{r_i r_j} .$$

For irrotational fluid, the transverse velocity correlation function, $\Sigma(r)$, and the parallel one, $\Pi(r)$, are interrelated via

$$\Pi(r) = \frac{\partial r \Sigma(r)}{\partial r} , \tag{13}$$

and the dot (total) velocity correlation is given by (e.g., Gorski 1988)

$$\Pi(r) + 2\Sigma(r) = v(r) . \tag{14}$$

Equations (10), (13), and (14) allow one to evaluate both components:

$$\Sigma(r) = \frac{1}{3} v(0) - H_0^2 \frac{\Omega^{1.2}}{b^2} \left[ \frac{1}{3} J_2(r) - \frac{1}{2} \frac{J_3(r)}{r} + \frac{1}{6} \frac{J_5(r)}{r^3} \right], \tag{15}$$

$$\Pi(r) = \frac{1}{3} v(0) - H_0^2 \frac{\Omega^{1.2}}{b^2} \left[ \frac{1}{3} J_2(r) - \frac{1}{3} \frac{J_5(r)}{r^3} \right]. \tag{16}$$

Now note that the quantity $\Sigma(r) - \Pi(r)$ is independent of the (a priori unknown) integration constant $v(0)$, and hence, once measured, it can provide a tool for measuring $\Omega^{0.6}/b$. It is given by

$$\Sigma(r) - \Pi(r) = H_0^2 \frac{\Omega^{1.2}}{b^2} \left[ \frac{1}{2} \frac{J_3(r)}{r} - \frac{1}{2} \frac{J_5(r)}{r^3} \right]. \tag{17}$$

Since the logarithmic slope of $\xi(r)$ is greater than $-2$, the expression on the right-hand side of equation (17) is dominated by the contribution from the integrands in $J_3$, $J_5$ near $r$. Therefore, for this quantity it is sufficient to choose a large enough separation to ensure the validity of the linear approximation.

For a power law $\xi(r) = (r/r_*)^{-1-\gamma}$, one gets

$$[\Sigma(r) - \Pi(r)]^{1/2} = \frac{\Omega^{0.6}}{b} \frac{H_0 r_*}{[(2-\gamma)(4-\gamma)]^{1/2}} \left( \frac{r}{r_*} \right)^{(1-\gamma)/2} \simeq 400\text{–}500 \text{ km s}^{-1}$$

for $\gamma = 0.7$ if $\Omega^{0.6}/b \simeq 1$. Figure 6 shows the predicted $[\Sigma(r) - \Pi(r)]^{1/2}$ in km s$^{-1}$ for $\Omega^{0.6}/b = 1$. The lines were evaluated using the CfA and APM data on $\xi(r)$; the notation is the same as in Figure 5. Again there is good agreement between the

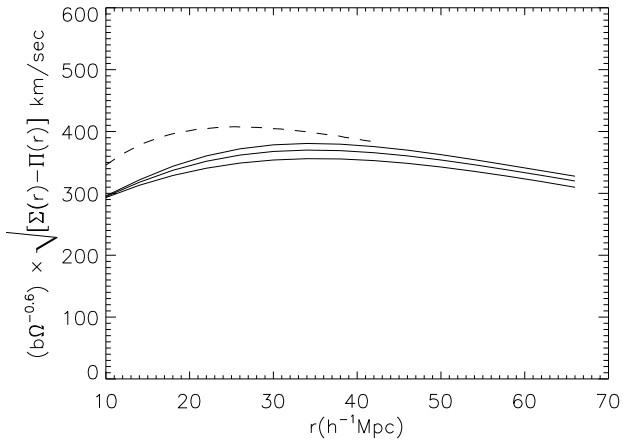


FIG. 6.—Values of the transverse minus parallel velocity correlations according to the data on $\xi(r)$. Same notation as in Fig. 5.

values computed from the "locally" determined correlation function (CfA; *dashed line*) and the "global" $\xi(r)$ from the APM data. The amplitude in Figure 6 scales $\propto\Omega^{0.6}/b$ and is quite significant if $\Omega^{0.6}/b \approx 1$. The data from previous analyses trying to reconstruct the velocity correlation tensor (Gorski et al. 1989; Groth, Juszkiewicz, & Ostriker 1989) from (by now old) catalogs are too uncertain to use in comparison with Figure 6. But the magnitude of $[\Sigma(r) - \Pi(r)]^{1/2}$ of $\sim 400$ km s$^{-1}$ over the range 30–60 $h^{-1}$ Mpc if $\Omega^{0.6}/b \simeq 1$ suggests that this could be a measurable task with the new data sets, and that in conjunction with the galaxy correlation data might further contrain $\Omega^{0.6}/b$.

Thus, the analysis and results of this section suggest the following:

1. The spectrum of mass distribution from velocity data is consistent with that determined from the galaxy correlation data (cf. Kashlinsky 1992b).
2. This in turn suggests that the bias factor is consistent with being scale independent.
3. Low values of $\Omega^{0.6}/b$ may be consistent with the data on peculiar velocities.
4. Thus, we interpret the results in Figure 4 as the rms density fluctuation of the pregalactic mass density field on scales $r_8 < r < 100\,h^{-1}$ Mpc.

## 5. CLUSTER CORRELATION FUNCTION AND ITS RICHNESS DEPENDENCE: RECONSTRUCTING PREGALACTIC SPECTRUM ON SCALES 5–25 $h^{-1}$ Mpc

The cluster-cluster correlation function is known to have a larger amplitude than the one measured by galaxies, and its amplitude also increases with the cluster richness (Bahcall & Soneira 1983). Kaiser (1984) suggested that the increase in the amplitude can be explained if clusters formed at the rare peaks of the initial density field. His analysis was later applied by Bardeen et al. (1986), to study in great detail the properties of peaks in the density field. Kashlinsky (1987, 1991*b*) proposed that one can combine Kaiser's original suggestion with gravitational clustering theory (Press & Schechter 1974) to explain both the amplification and its correlation with the cluster richness. He supposed that structure formation in the universe forms via a "natural bias" (cf. Davis et al. 1985), i.e., systems of galaxies (clusters and groups) should be identified with regions that had turnaround time less than the age of the universe. The model successfully explained the correlation between the cluster correlation function and richness (mass) with objects that turned around on a larger scale having a greater correlation amplitude.

Within the gravitational clustering model, the properties of the hierarchy would then depend uniquely upon the *initial* power spectrum and the mass of the objects that formed/turned around. In this section we first evaluate in greater detail the predicted properties of the cluster correlation function according to the gravitational clustering picture (Kashlinsky 1987, 1991*b*), and then apply the results to invert the data on the cluster correlation function to obtain the *pregalactic* spectrum of the density field on scales $5\,h^{-1}$ Mpc $< r < 20\,h^{-1}$ Mpc.

We start with the density field at some initial epoch, $z_i \gg 1$, when density fluctuations were linear on all scales of interest. The final results will be independent of $z_i$. We define with $\delta_M = \int \delta(\mathbf{x})dV/\int dV$ the initial mass overdensity over the comoving volume $V$ that contains mass $M$. On large scales, $r \gg R(M)$, where $R(M)$ is the comoving scale containing mass $M$, the correlation function of the $\delta_M$ field coincides with $\xi(r)$. At zero lag, it equals the mean square fluctuation over mass $M$: $\Delta_i^2(M) = \langle \delta_M^2 \rangle$; the subscript $i$ refers to the values evaluated at $z_i$. Thus, the correlation matrix for the $\delta_M$ field is

$$\{C_{lm}\} = \begin{pmatrix} \Delta_i^2(M) & \xi_i(r) \\ \xi_i(r) & \Delta_i^2(M) \end{pmatrix}. \tag{18}$$

We assume that the *initial* density field was Gaussian. Then the probability density to find two regions containing masses $M_1, M_2$ that had density fluctuations $\delta_1, \delta_2$ at $z_i$ is

$$p(\delta_1;\, \delta_2) = \frac{1}{2\pi\|\boldsymbol{C}\|} \exp\left(-\frac{1}{2}\,\boldsymbol{\delta}\cdot\boldsymbol{C}^{-1}\cdot\boldsymbol{\delta}\right). \tag{19}$$

As the clustering evolves, deviations from Gaussianity will develop due to gravitational effects. However, since we trace the distribution of the prospective clusters at $z_i$, these will not be important for the computation of the cluster correlation function below. Using properties of the Fourier transform of a multidimensional Gaussian, equation (19) can be rewritten in terms of the direct matrix $\boldsymbol{C}$ as

$$p(\delta_1;\,\delta_2)=\frac{1}{(2\pi)^2}\int_{-\infty}^{\infty}\int_{-\infty}^{\infty}\exp\left(-i\boldsymbol{q}\cdot\boldsymbol{\delta}\right)\exp\left(-\frac{1}{2}\,\boldsymbol{q}\cdot\boldsymbol{C}\cdot\boldsymbol{q}\right)d^2q\;. \tag{20}$$

We denote by $\delta_{\rm ta}$ the amplitude at $z_i$ required for the fluctuation to turn around at $z=0$ and use the Press-Schechter (1974) prescription for gravitational clustering, which assumes that any region with $\delta_M\geq\delta_{\rm ta}$ would have turned around by now. We further assume that clusters and groups of galaxies are identified with such regions. Then the probability for two clusters of masses $M_1$ and $M_2$ to have formed at any time between now and $z_i$ is given by integrating equation (2) over all fluctuations $\geq\delta_{\rm ta}$. We denote with $\Delta_{8,i}$ the amplitude the fluctuation had to have on scale $r_8$ at $z_i$ in order to grow to the observed value of $1/b$ at $z=0$. A convenient way to characterize $\delta_{\rm ta}$ and to normalize the density field is by introducing the quantity $Q_{\rm ta}=\delta_{\rm ta}/\Delta_{8,i}$ (Kashlinsky 1991*b*). For $\Delta_8=1$ today, $Q_{\rm ta}\simeq 1.65$ almost independently of $\Omega$ or $z_i$, We adopt this value of $Q_{\rm ta}$ in the calculations of this section. We will show that this set of "minimal assumptions," including $b=1$, is justified, since it gives a fit to the derived spectrum consistent with the APM data.

Expanding in equation (20)

$$\exp\left(-\frac{1}{2}\,\boldsymbol{q}\cdot\boldsymbol{C}\cdot\boldsymbol{q}\right)=\sum_{m=0}^{\infty}\frac{(-)^m}{m!}\,q_1^m\,q_2^m\,\xi_i^m\exp\left[-\frac{q_1^2\,\Delta^2(M_1)}{2}\right]\exp\left[-\frac{q_2^2\,\Delta^2(M_2)}{2}\right],$$

we can write the probability for two clusters of mass $M_1$ and $M_2$ to form at any time between $z_i$ and $z=0$ as

$$P_{M_1M_2}=\int_{\delta_{\rm ta}}^{\infty}\int_{\delta_{\rm ta}}^{\infty}p(\delta_1,\,\delta_2)d\delta_1\,d\delta_2=\frac{1}{2\pi^2}\sum_{m=0}^{\infty}\frac{(-)^m}{m!}\left[\frac{\xi_i}{\Delta_i(M_1)\Delta_i(M_2)}\right]^m a_m(\zeta_1)a_m(\zeta_2)\;, \tag{21}$$

where

$$a_m(\zeta)=\int_{\zeta}^{\infty}dx\int_{-\infty}^{\infty}y^m\exp\left(-ixy\right)\exp\left(-\frac{y^2}{2}\right)dy\;. \tag{22}$$

The quantity $\zeta$ is the number of standard deviations that cluster of mass $M$ is with respect to the "typical" member of the hierarchy, and is given by

$$\zeta=Q_{\rm ta}\,\frac{\Delta_8}{\Delta(M)}=Q_{\rm ta}\left[\frac{\int_0^{\infty}P(k)W_{\rm TH}(kr_8)k^2\,dk}{\int_0^{\infty}P(k)W_{\rm TH}(kR(M))k^2\,dk}\right]^{1/2}\;, \tag{23}$$

where $R(M)$ is the scale containing mass $M$. The power spectrum in equation (23) is the original *pregalactic* power spectrum of the density field.

In order to directly evaluate $P_{M_1M_2}$ and the cluster correlation function, we write

$$\int_{-\infty}^{\infty}\exp\left(-ixy-\frac{1}{2}\,y^2\right)y^m\,dy=i^m\,\frac{\partial^m}{\partial x^m}\int_{-\infty}^{\infty}\exp\left(-ixy-\frac{1}{2}\,y^2\right)dy=i^m(2\pi)^{1/2}\,\frac{\partial^m}{\partial x^m}\exp\left(-\frac{1}{2}\,x^2\right)$$

(Jensen & Szalay 1986). Then equations (21) and (22) become

$$P_{M_1M_2}=\frac{1}{2\pi}\sum_{m=0}^{\infty}\frac{1}{m!}\left[\frac{\zeta_i}{\Delta_i(m_1)\Delta_i(M_2)}\right]^m\left[\frac{\partial^{m-1}\exp\left(-\zeta_1^2/2\right)}{\partial\zeta_1^{m-1}}\right]\left[\frac{\partial^{m-1}\exp\left(-\zeta_2^2/2\right)}{\partial\zeta_2^{m-1}}\right]. \tag{24}$$

The probability for a cluster of mass $M$ to form by now, is for a Gaussian ensemble, given by

$$P_M=\frac{1}{2}\,\mathrm{erfc}\left(\frac{\zeta}{\sqrt{2}}\right). \tag{25}$$

Equations (24) and (25) give the cumulative probability of objects to turn around at any time in the past. In the gravitational clustering picture, $P_M$'s include objects that formed at earlier epochs and by now are incorporated into larger systems. Because clusters and groups form without dissipation, the objects that formed earlier would merge into larger systems and lose their identity as clustering progresses to larger masses. Since we observe at a fixed epoch ($z=0$), one must translate equations (24) and (25) into probabilities that the objects formed (turned around) today. Thus, the fraction of pairs of clusters that formed today on mass scales $M_1$, $M_2$ separated by distance $r$ out of the ensemble of density fluctuations given by equation (19) is $f_{M_1M_2}=\partial^2P_{M_1M_2}/\partial M_1\partial M_2$. Similarly, the fraction of clusters in the mass range $[M,\,M+dM]$ is $f_M\,dM=(\partial P_M/\partial M)dM$ (Press & Schechter 1974). From equations (24) and (25) one can show that

$$\frac{f_{M_1M_2}}{f_{M_1}\,f_{M_2}}=\frac{\partial^2P_{M_1M_2}}{\partial\zeta_1\partial\zeta_2}\Bigg/\frac{\partial P_{M_1}}{\partial\zeta_1}\,\frac{\partial P_{M_2}}{\partial\zeta_2}=\sum_{m=0}^{\infty}\frac{1}{Q_{\rm ta}^{2m}\,m!}\left(\frac{\zeta i}{\Delta_8^2}\right)^m B_m\left(\frac{\zeta_1}{\sqrt{2}}\right)B_m\left(\frac{\zeta_2}{\sqrt{2}}\right), \tag{26}$$

where $B_m(x) = \frac{1}{2}x^{m-1}H_{m+1}(x)$ (Kashlinsky 1991*b*) and

$$H_n(x) = (-)^n \exp(x^2) d^n[\exp(-x^2)]/dx^n$$

are the Hermite polynomials. We will be using the measurements of the cluster correlation function on linear scales, $r > r_8$. On these scales, the ratio on the right-hand side of equation (26), $\xi_i/\Delta_8^2$, where both the numerator and denominator are evaluated at $z_i$, is roughly independent of redshift and is approximately equal to the galaxy correlation function today, $\xi(r)$.

Having fixed the fractions of objects that turned around today on a given scale, we can evaluate the correlation function between clusters of different masses $\xi_{M_1M_2}$. By definition, the two-point correlation function of an ensemble of objects with number density $n$ is given by the probability of finding two objects in small volumes $dV_1$, $dV_2$ as $d\mathscr{P}_{12} = n^2(1 + \xi)\, dV_1\, dV_2$. Since the clusters of mass $M_1$ and $M_2$ make the fraction $f_{M_1M_2}$ of such pairs, the probability of finding them is $d\mathscr{P}_{M_1M_2} = f_{M_1M_2}\, d\mathscr{P}_{12}$. On the other hand, the mean number density of clusters of mass $M$ would be $f_M \times n$, and by definition the probability of finding two clusters is $d\mathscr{P}_{M_1M_2} = f_{M_1} f_{M_2} n^2(1 + \xi_{M_1M_2}) dV_1\, dV_2$. Hence the correlation function of clusters of mass $M$ is given by

$$1 + \xi_{M_1M_2} = \frac{f_{M_1M_2}}{f_{M_1} f_{M_2}}(1 + \xi_i) = (1 + \xi_i)\frac{\partial^2 P_{M_1M_2}}{\partial\zeta_1\partial\zeta_2}\Big/\frac{\partial P_{M_1}}{\partial\zeta_1}\frac{\partial P_{M_2}}{\partial\zeta_2}\,. \tag{27}$$

Equation (27) fixes the factor by which the cluster correlation function is amplified over the underlying correlation function of the hierarchy, $\xi$. The amplification is purely statistical, and the discussion does not involve any dynamical effects. Hence, on linear scales today the amplification factor $\xi_{MM}/\xi_i$ is redshift independent, and for $r > r_8$ the present-day correlation function for clusters of mass $M$ should be amplified over $\xi(r)$ according to

$$\xi_{MM}(r) = A_M\left(\frac{\zeta}{\sqrt{2}}\right)\xi(r)\,, \tag{28}$$

where

$$A_M(x) = \sum_{m=0}^{\infty}\frac{1}{Q_{\rm ta}^{2m} m!}\,\xi^m C_M(x)\,, \tag{29}$$

and

$$C_m(x) = \frac{x^{2m}}{4}\left[\frac{H_{m+1}^2(x)}{x^2} + \frac{H_{m+2}^2(x)}{(m+1)Q_{\rm ta}^2}\right]. \tag{30}$$

In evaluating equation (28)–(30) we used the fact that the ratio $\xi_i/\Delta_{8,i}$ evaluated at $z_i$ for scales $r > r_8$ is $\simeq\xi(r)$, the galaxy two-point correlation function that is measured today. As $x \to 0$, equation (30) gives $C_0 \to 1$, and one gets from the first term in equation (28) that, at small $\xi(r)$, $\xi_{MM}(r) \simeq \xi(r)$. For large masses or $x \gg 1$, the first term in equation (29) is $C_0 = \zeta^4$ and the amplification reduces to $\xi_{MM}(r) \simeq Q_{\rm ta}^4[\Delta_8/\Delta(M)]^4\xi(r)$ (cf. Kashlinsky 1987). (The quantity $Q_{\rm ta}$ in this discussion is equivalent to the threshold amplitude $b$ of Kaiser 1984).

Equations (28)–(30) show that the spectrum of the pregalactic density field can be constrained, and, as we show later, determined, by the data on both the slope of the observed cluster correlation function $\xi_{CC}(r)$ via equation (28), and the dependence of the amplitude on the cluster mass via equation (29). Bahcall & Soneira (1983) present the data on both of these for scales greater than $r_8$ where the present analysis applies. The slope of the cluster correlation function on very large scales, $r > 50\ h^{-1}$ Mpc, is poorly determined from the data (cf. Fig. 9 of Bahcall & Soneira 1983). For richness class $\mathscr{R} \geq 1$ Abell clusters, such as Coma, they approximate $\xi_{\rm CC}(r) \simeq 300(r/1\ h^{-1}\ {\rm Mpc})^{-1.8}$. This approximation has large uncertainty at large scales, but for $r < (30\text{–}40)\ h^{-1}$ Mpc, it can be used as a reasonable approximation to the data. The Zwicky clusters, which are poorer, also exhibit a stronger correlation amplitude than galaxies (Postman et al. 1986), although it is weaker than that of Abell clusters and is consistent with the amplitude-richness relation proposed in Bahcall & Soneira (1983). Figure 2 in Bahcall & West (1992) shows the largest compilation of the data on cluster correlation amplitude versus richness. Thus we use below the data on the cluster correlation function from Bahcall & Soneira (1983) and on the richness–correlation amplitude dependence for clusters of galaxies from Bahcall & West (1992).

In order to compare equations (28)–(30) with the data discussed above, we must fix the mass of the clusters quantitatively. We use Coma, the best-studied cluster, as the mass normalization point. From Kent & Gunn (1981), we adopt its mass to be $M_{\rm Coma} = 1.45 \times 10^{15}\ h^{-1}\ M_\odot$ (see also White et al. 1993 and references cited therein). The richness of the Coma Cluster is adopted from Bahcall (1981) and Abell et al. (1989) to be $\mathscr{N}_{\rm Coma} = 106$. Assuming that both the luminosity function of galaxies and the ratio of dark to luminous matter are universal for all clusters would imply that the cluster richness is proportional to mass. We thus adopt the following relation between cluster mass and richness:

$$M = M_{\rm Coma}\frac{\mathscr{N}}{\mathscr{N}_{\rm Coma}} = 1.45 \times 10^{15}\left(\frac{N}{106}\right) h^{-1}\ M_\odot\,, \tag{31}$$

while the comoving scale containing mass $M$ that enters in the integrand of the denominator in equation (23) is given by

$$R(M) = 0.2\left(\frac{M}{10^{10}\ h^{-1}\ M_\odot}\right)^{1/3}\Omega^{-1/3}\ h^{-1}\ {\rm Mpc}\,. \tag{32}$$

We can now move to the implications of the cluster correlation data for the spectrum of the pregalactic density field. For a given $P(k)$, equations (3) and (23) specify $\xi(r)$ and $\Delta(M)/\Delta_8$, which in turn uniquely determine both the cluster correlation function as a function of $r$ and its amplitude as a function of the mass computed from the cluster richness according to equation (31). For CDM models, the value of $\Omega h$ is not the only parameter that fixes the cluster correlation function; the extra dependence on $h$ comes from translating the mass scales to linear scales via equation (32). Figure 7 plots the cluster correlation in CDM models with the Harrison-Zeldovich power spectrum, $n = 1$, for various $\Omega$ and $h$. Thin solid lines correspond to the underlying correlation function, $\xi(r)$, for given $\Omega$, $h$. Thick solid lines correspond to the $\xi_{CC} = 300(r/1\ h^{-1}\ \mathrm{Mpc})^{-1.8}$ that Bahcall & Soneira (1983) find for $\mathscr{R} \geq 1$ clusters. The numbers are plotted between 20 and 100 $h^{-1}$ Mpc, where the galaxy correlation function is in the linear regime and is thus given by the pregalactic power spectrum. Dotted lines correspond to $\mathscr{N} = 5$, dashes to $\mathscr{N} = 10$, dash-dotted lines to $\mathscr{N} = 50$, and dash-dot-dotted lines to clusters such as Coma, $\mathscr{N} = 100$. Successful models should fit both the amplitude and the slope of the measured $\xi_{CC}$, while at the same time the underyling $\xi(r)$ should be in agreement with the APM data constraints in Figure 3. As one can see from the figure, the required increase in the amplitude for clusters of richness class $\mathscr{R} \geq 1 (\mathscr{N} \simeq 100)$ can be achieved for $\Omega \sim 0.3$–$0.4$, but such models would not reproduce the observed slope of $\xi_{CC}(r)$, even on scales $\lesssim 30$–$40\ h^{-1}$ Mpc where the data are more reliable and are definitely not expected to be subject to possible projection effects (Sutherland 1988). The required slope of $\xi_{CC}(r)$ can be reproduced for $\Omega = 0.1$ and $h = 0.5$, but then the observed amplitude would be reached for $\mathscr{N} = 10$, corresponding to poor groups, while clusters such as Coma should have correlation amplitudes significantly above that observed. Furthermore, such models with $\Omega h \simeq 0.05$ would have values for $\theta(w = 5 \times 10^{-3})$—plotted with asterisks in Figure 3—that are much larger than the values deduced from the APM data. For brevity we do not present the same graph for $h = 1$, but the agreement with the measurements would become even worse for $h > 0.5$.

Figure 8 plots the predicted $\xi_{MM}(r)$ for tilted CDM models with $n = 0.7$; the line notation is the same as in Figure 7. The tilted CDM model also does not fit well the data on the cluster correlation function or the APM data. For example, the model can reasonably reproduce the slope and the amplitude of Abell clusters if $\Omega = 0.3$, $h = 0.5$, but then with $\Omega h \simeq 0.15$. it would predict $\theta(w = 5 \times 10^{-3})$ in Figure 3 far above the APM data.

In order to illustrate the dependence of the amplitude on mass or richness for CDM models, we computed the amplification factor, equation (29), at $r = 25\ h^{-1}$ Mpc. This scale is $\gg r_8$, so it is reasonable to suppose that the density field there reflects the pregalactic density field. At the same time, on this scale the underlying $\xi(r)$ is still positive in all relevant CDM models. Figure 9 plots the values of $A(25\ h^{-1}\ \mathrm{Mpc})$ versus the cluster richness for CDM models. The right-hand panel shows the numbers for $n = 1$, and the left-hand panel shows them for tilted CDM models. Triangles correspond to the data from Figure 3 of Bahcall & West (1992). Solid lines correspond to $\Omega h = 0.1$, dotted lines to $\Omega h = 0.2$, dashed lines to $\Omega h = 0.3$, and dash-dotted lines to $\Omega h = 0.5$. Thin lines of each type are for $h = 1$, and thick lines are for $h = 0.5$.

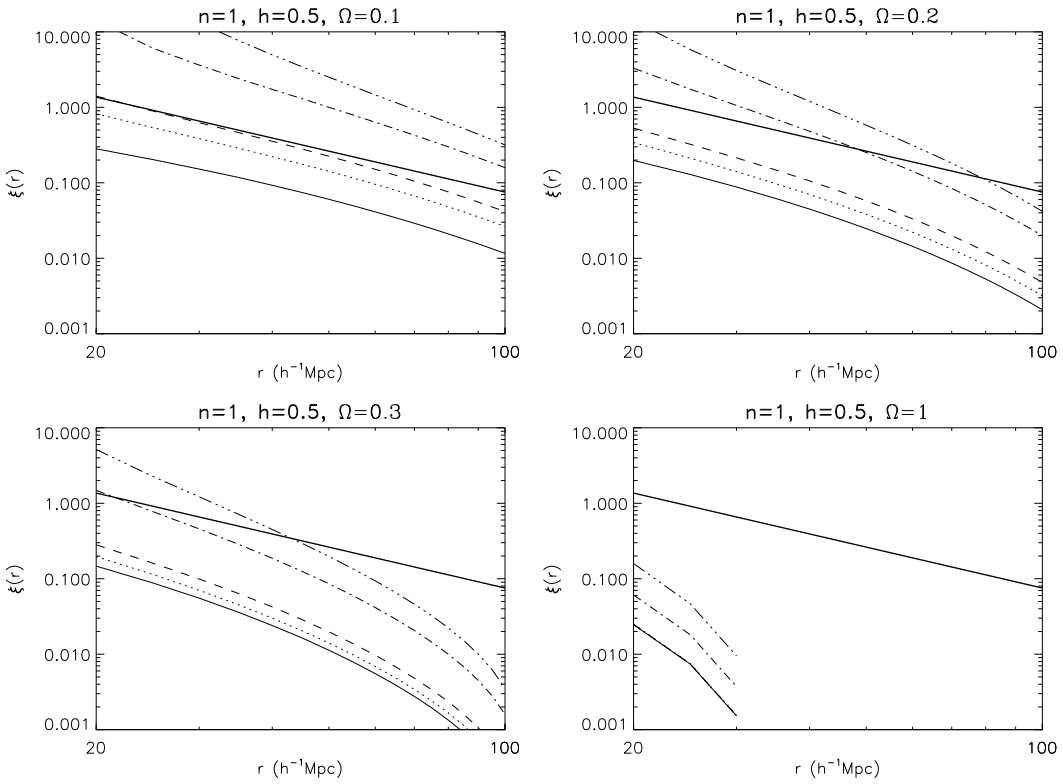


FIG. 7.—Cluster-cluster correlation function for CDM models with $n = 1$ and various $\Omega$, $h$ on scales $20\ h^{-1}\ \mathrm{Mpc} < r < 100\ h^{-1}\ \mathrm{Mpc}$. Thin solid lines show the underlying correlation function in the CDM model specified on top of each panel. Dotted lines show the amplified correlation function for clusters of richness $\mathscr{N} = 5$, dashes for clusters with $\mathscr{N} = 10$, dash-dotted lines to $\mathscr{N} = 50$, and the dash-double-dotted lines to $\mathscr{N} = 100$. For comparison, the richness class $\mathscr{R} \geq 1$ clusters, such as Coma, have $\mathscr{N} = 100$. The thick solid line corresponds to the approximation $\xi_{CC} = 300(r/1\ h^{-1}\ \mathrm{Mpc})^{-1.8}$, which Bahcall & Soneira (1983) find for $\mathscr{R} \geq 1$ clusters.

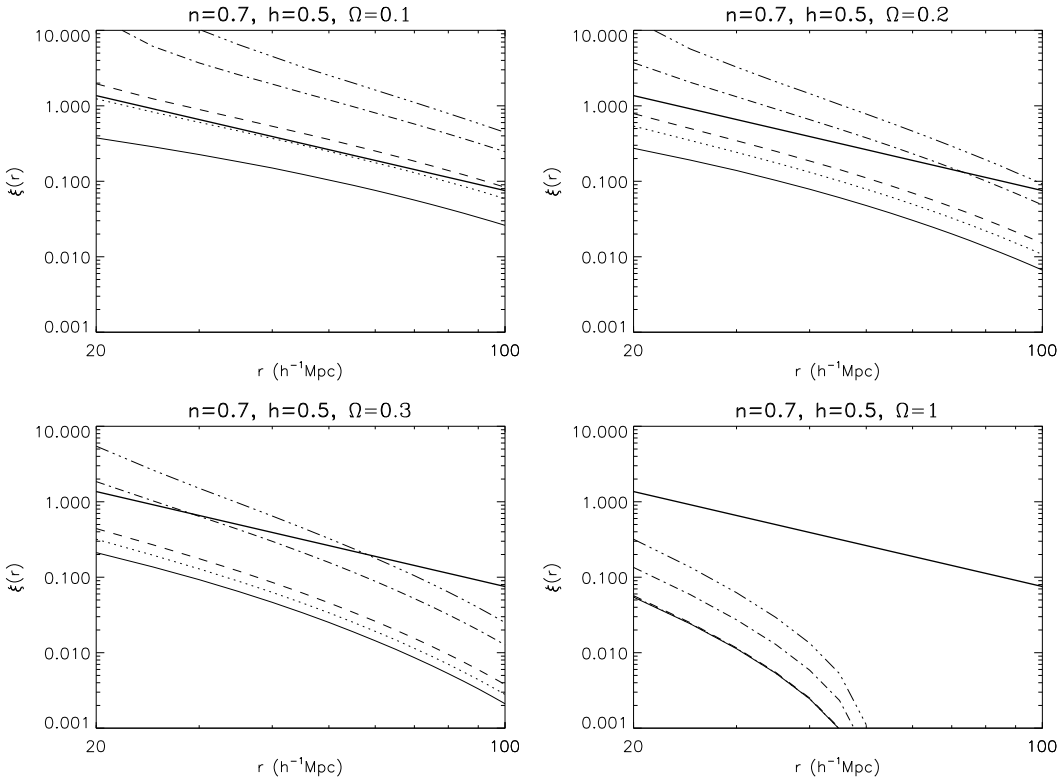


FIG. 8.—Same as Fig. 7, but only for tilted CDM models with $n = 0.7$. Same notation as in Fig. 7.

One can see that it is difficult to describe all the data with one particular CDM model. In other words, the slope of the pregalactic power spectrum over different ranges of scales as probed by Figures 7–9 cannot be fitted with one formula given by equation (2) for any value of $\Omega$, $h$, or $n$. Further difficulty would come from constraining the CDM models to fit the APM data along with the cluster correlation data. As Figure 3 shows, CDM models would be consistent with APM data only if $\Omega h \simeq 0.2$ for $n = 1$ and $\Omega h \simeq 0.3$ for $n = 0.7$. This would further restrict the models to dotted lines in the left-hand panel of Figure 9 and to dashed lines in the right-hand panel.

One can now reverse the problem, and instead of fitting various theoretical models to the cluster correlation amplitude–richness data, one can invert the data to *obtain the implied pregalactic density spectrum from equation (29) with x given by equation (23)*. This can be done if one uses independent measurement of the underlying correlation function, $\xi(r)$, in the linear regime. Then the latter can be substituted in equation (29) with $x$ given by equation (23), to give an equation after solving which one can determine, for given measurements of $A(M)$ versus richness for clusters, the values of $\Delta(M)\Delta_8$ of the pregalactic density field on mass scale $M$ (in turn given by equation [31]).

First we consider the choice of scale $r$ on which the data on $\xi(r)$ are to be used. Such a scale must be greater than $r_8$, since $\xi(r)$ in equation (29) is given by the pregalactic power spectrum at $z_i$. Figure 10 plots $\xi(r)$ from the various fits to the APM data. Solid lines are the K92 fits with $k_0^{-1} = 35$, 40, and 50 $h^{-1}$ Mpc from bottom to top. Dotted lines are for the BE93 fit with top and bottom lines corresponding to the 1 standard deviation uncertainty. For comparison, we also plot with dashed lines

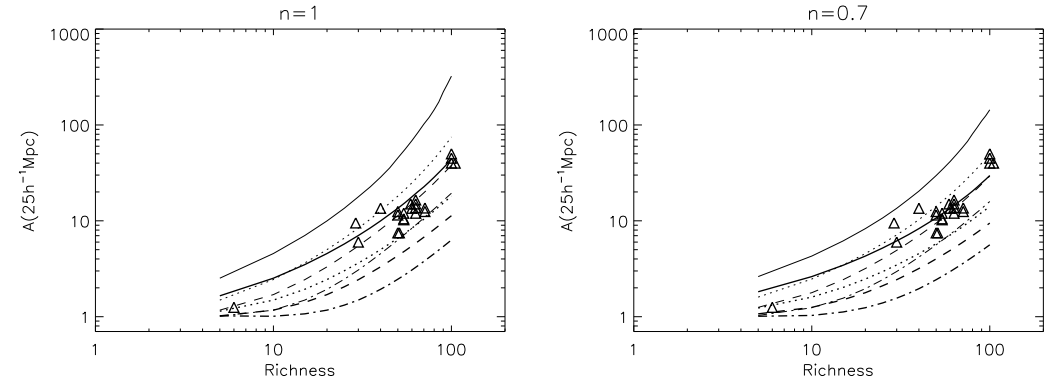


FIG. 9.—Amplification of the correlation function for clusters $A = \xi_{MM}(r)/\xi(r)$ evaluated for CDM models at $r = 25\ h^{-1}$ Mpc plotted vs. cluster richness. Triangles correspond to the data points from Fig. 3 of Bahcall & West (1992). Solid lines are for CDM models with $\Omega h = 0.1$, dotted lines for $\Omega h = 0.2$, dashed lines for $\Omega h = 0.3$, and dash-dotted lines for $\Omega h = 0.5$. Thin lines of each type are for $h = 1$, and thick lines are for $h = 0.5$.

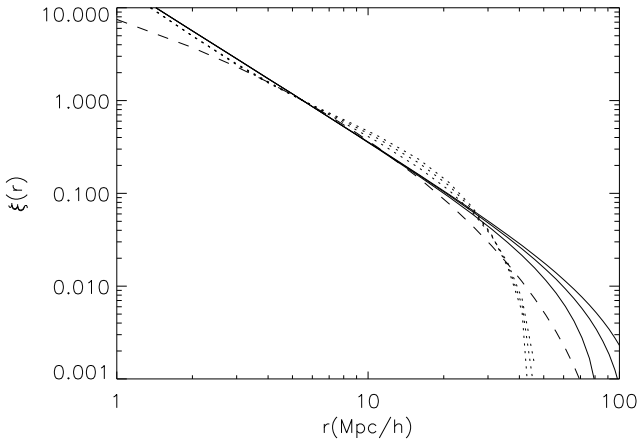


FIG. 10.—Correlation function $\xi(r)$, according to the various fits to APM, plotted vs. $r$. Dashed line corresponds to a CDM model with $n = 1$ and $\Omega h = 0.2$ or $n = 0.7$ and $\Omega h = 0.3$ (the two practically coincide). Dotted lines correspond to the BE93 fit with 1 standard deviation uncertainty. Three solid lines correspond to the K92 fit with the transition scale $k_0^{-1} = 35, 40, 50\ h^{-1}$ Mpc.

the correlation function according to CDM models (equation 2) with $n = 1$ for $\Omega h = 0.2$ (the $n = 0.7$ and $\Omega h = 0.3$ line would essentially coincide with the thick line over the linear scales; hence it is not plotted). All the fits to the APM data give essentially the same $\xi(r)$ between 10 and 30 $h^{-1}$ Mpc. Thus, we choose the scale $r = 25\ h^{-1}$ Mpc for which to substitute the measured $\xi(r)$ into equation (29). The latter is sufficiently larger than $r_8$ to be certain that $\xi(r)$ there reflects the pregalactic density field and, at the same time, sufficiently small so that the cluster correlation amplitude measurements are free from the possible uncertainties at larger scales. Using the data on $r$ anywhere between 15 and 30 $h^{-1}$ Mpc would introduce little difference in the results to come. From Figure 10 we adopt this scale $r = 25\ h^{-1}$ Mpc with the measured correlation function there $\xi(25\ h^{-1}\ \text{Mpc}) = 0.07$. The same number would be given also by a simple power extrapolation of $\xi(r) = (r/r_*)^{-1.7}$ to $r = 25\ h^{-1}$ Mpc.

The solid line in Figure 11 plots the amplification factor $A(x)$ at 25 $h^{-1}$ Mpc versus $x$ according to equation (29) after adopting $\xi(25\ h^{-1}\ \text{Mpc}) = 0.07$. One can see that at small $x$ (small mass scales) $A(x)$ has a very weak dependence on $x$. Hence, for small mass scales, the determination of $x$, or $\Delta(M)/\Delta_8 = Q_{\text{ta}}/x\sqrt{2}$, is less accurate since the errors in the data will amplify. On the other hand, at large $x$ the dependence is quite steep, and the determined spectrum will be less sensitive to observational errors in cluster correlation measurements for massive clusters. Note that the first term (and leading term at large $x$ and small $\xi$) in equation (29) is independent of $\xi(r)$. The two dotted lines show the uncertainty in $A(x)$ introduced by assuming, for example, a 25% uncertainty in the value of $\xi$, i.e., the lines plotted cover the range of $0.05 < \xi(25\ h^{-1}\ \text{Mpc}) < 0.1$. One can see that the values of $\Delta(M)/\Delta_8$ determined in this way depend very weakly on the possible uncertainties in $\xi(r)$.

We now use the data from Figure 3 of Bahcall & West (1992), plotted with triangles in Figure 9 in order to invert equation (29), with $\xi(25\ h^{-1}\ \text{Mpc}) = 0.07$, to give $\Delta(M)/\Delta_8$ of the pregalactic density field on scale $M$, or richness $\mathcal{N}$. Figure 12 plots the results of this inversion. The top horizontal axis plots the values of $\mathcal{N}$ at which $\Delta(M)/\Delta_8$ has been evaluated. The bottom horizontal axis shows the mass computed according to the normalization given by equation (31). We emphasize again that this method gives directly the pregalactic spectrum as it was at $z_i$ independent of the later gravitational or other effects. The plot in Figure 12 shows a clearly defined slope of $\Delta(M) \propto M^{-0.275}$ corresponding to the spectral index of $n \simeq -1.3$. This slope is consistent with the APM implied power spectrum index of $w(\theta) \propto \theta^{-0.7}$.

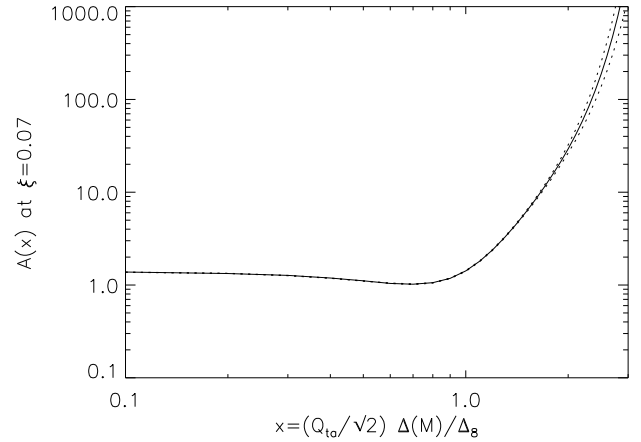


FIG. 11.—The amplification factor $A(x)$ is plotted according to eq. (29). The solid line corresponds to the underlying correlation $\xi = 0.07$, and the two dotted lines show the results of, say, 25% uncertainty in $\xi$.

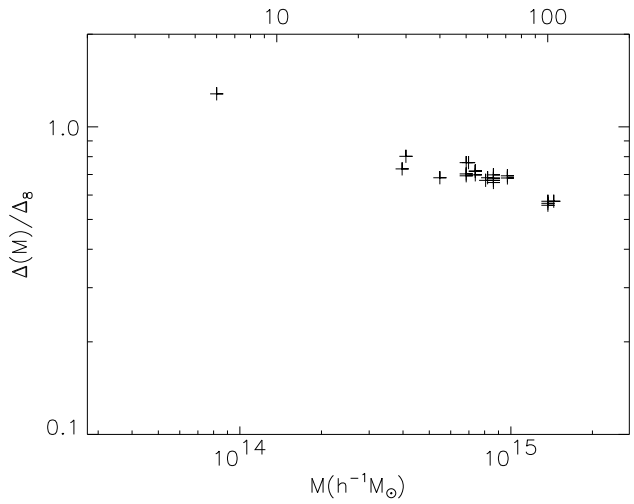


FIG. 12.—Spectrum of the pregalactic density field, $\Delta(M)/\Delta_8$, obtained from the data on the cluster correlation amplitude–richness dependence. The upper horizontal axis shows the richness corresponding to the particular value of $\Delta(M)/\Delta_8$. The lower horizontal axis shows the values of $M$ computed from normalization to Coma (eq. [31]).

Finally, we note that even if the underlying density field is purely Guassian, the distribution of clusters of galaxies would be non-Gaussian (Politzer & Wise 1984; Kashlinsky 1991*b*). Kashlinsky (1991*b*) analyzed the properties of the three-point function of clusters predicted by this model and found that they compare favorably with the measurements of the cluster three-point correlation function by Toth et al. (1989), assuming that the pregalactic power spectrum is close to $n \simeq -1$ on all scales below 100 $h^{-1}$ Mpc. In principle, one could apply similar methods to derive the properties of the pregalactic density field from the three-point correlation function of clusters of various richness/mass. The data available at present do not justify a lengthy addition on this subject to this paper, so we postpone this part of the discussion to a forthcoming paper.

## 6. COMBINING THE RESULTS FROM $w(\theta)$ AND $\xi_{CC}$: $\Omega$ AND THE PREGALACTIC DENSITY FIELD

The agreement of the slope of the spectrum in Figure 12 determined from the cluster correlation amplitude versus richness data with that deduced from the APM catalog is encouraging and shows the consistency of this approach. Furthermore, the APM data set fixes the spectrum of the pregalactic density on a given linear scale, $r$, while the method outlined in the previous section determines it on a given mass scale, $M$. The resultant spectra are consistent in slope, and requiring them to give identical amplitude at a given linear (or mass) scale could then constrain $\Omega$ via equation (32).

Figure 13 shows $\Delta(M)/\Delta_8$ from Figure 12 plotted as a function of the linear scale containing the mass on the lower horizontal axis of Figure 12. The linear scale $r$ in $h^{-1}$ Mpc was computed according to equation (32). The left-hand panel of Figure 13 shows the numbers for $\Omega = 1$ (*thick plus signs*) *and* $\Omega = 0.1$ (*thin plus signs*). The open square in the figure shows the value of 1 for $\Delta(M)/\Delta_8$ at $r_8$; for the pregalactic density field, this number must be unity *by definition.* Clearly $\Omega = 1$ would be difficult to reconcile with $\Delta(M)/\Delta_8 = 1$ at $r_8$; extrapolating from *all* the data points misses the square by a significant factor. A value of $\Omega < 1$ would be required to reproduce the unity value for $\Delta(M)/\Delta_8$ at $r_8$, as obtained from the cluster correlation amplitude versus richness dependence.

We now use equation (32) to determine $\Omega$ by requiring the pregalactic density field derived from the cluster correlation function to match that derived from the APM data on the same scales. The right-hand panel of Figure 13 shows the

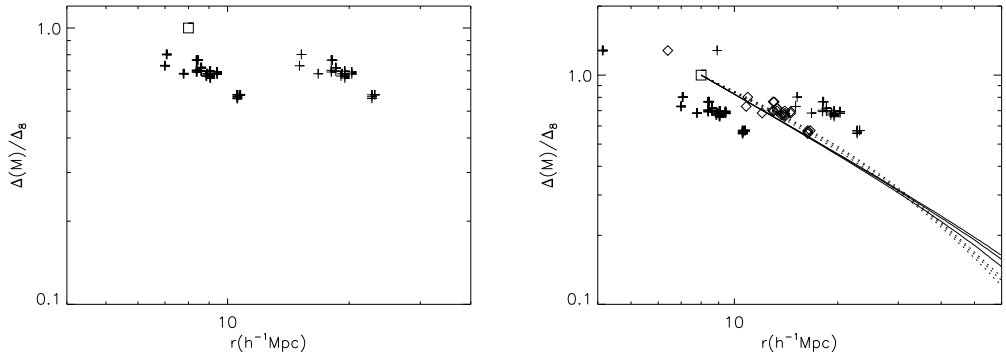


FIG. 13.—Plots $\Delta(M)/\Delta_8$ from Fig. 12 vs. linear scale (eq. [32]). In the left-hand panel thick plus signs correspond to $\Omega = 1$ and thin plus signs correspond to $\Omega = 0.1$. The open box corresponds to $\Delta(M)/\Delta_8 = 1$ at $r = 8$ $h^{-1}$ Mpc; the numbers miss this point if $\Omega = 1$. In the right-hand panel, dotted lines correspond to the BE93 fit to the APM data with 1 standard deviation uncertainty. Solid lines are for K92 fit with transition scale $k_0^{-1} = 35, 40, 50$ $h^{-1}$ Mpc. Diamonds correspond to the data from Fig. 12 with $\Omega \simeq 0.25$ when it would coincide with the independently deduced lines from the APM data. Other signs are in the same notation as in Fig. 12.

intercomparison. The lines are in the same notation as in Figure 10: solid lines correspond to the K92 fit, and dotted lines correspond to the BE93 fit. The plus signs and square symbols correspond to the same notation as in the left-hand panel of the figure. The diamonds correspond to $\Omega = 0.25$, with which the best agreement between the $\Delta(M)/\Delta_8$ values derived from the cluster correlation amplitude and APM data set is achieved. Note that any deviations from spherical approximation will speed up the collapse (Peebles 1980) leading to a *smaller* value of $Q_{\rm ta}$. This will shift the values of $\Delta(M)/\Delta_8$ from the cluster correlation analysis that best fit APM data toward even lower values of $\Omega$.

It is interesting to note that the value of $\Omega = 0.25$ deduced in this analysis is in good agreement with that required by the dynamics of the Coma Cluster. This cluster is by far the best studied and was also used in the normalization of the mass-richness relation used in § 5. The blue mass-to-light ratio of the Coma Cluster is very accurately determined to be $M/L_B \simeq 362\ h$ in agreement with the value of $M_{\rm Coma}$ used in equation (31). If one adopts the blue luminosity function of the Schechter form $\Phi(L)dL = \Phi_*(L/L_*)^{-\alpha} \exp(-L/L_*)d(L/L_*)$ and assumes that the entire mass in the universe is associated with galaxies and their systems, the total mass-to-light ratio of galactic systems would be uniquely related to $\Omega$ via

$$\frac{M}{L_B} = \frac{3H_0^2}{8\pi G\Phi_* L_* \Gamma(2-\alpha)}\,\Omega = 1330h \quad (\Omega \text{ in solar units})\,, \tag{33}$$

where $\Gamma(x)$ is the gamma function. In equation (33) the numbers were evaluated using the data on the luminosity function from the latest APM survey of Loveday et al. (1992). Thus the dynamics of the Coma Cluster implies the same value of the density parameter that we find from the independent analysis in this section; assuming that the mass-to-light ratio of galaxies varies according to the fundamental plane of ellipticals will result in less than 10% correction, as will be discussed in the next section.

To conclude the sections on the cluster correlation function and the pregalactic density field:

1. We find that CDM models with any $\Omega$, $h$ cannot fit simultaneously the data on the slope of the cluster correlation function, the dependence of its amplitude on richness, and the APM angular correlation function.
2. We developed a method to determine the values of $\Delta(M)/\Delta_8$ of the pregalactic density field directly from the data on the cluster correlation amplitude versus richness. The values determined in this way are independent of the numerical value of the biasing factor.
3. The slope of the pregalactic density field, $\Delta(M)/\Delta_8$ versus the mass $M$, found in this way is consistent with that determined from APM.
4. Comparison of the amplitude of $\Delta(M)/\Delta_8$ on a given linear scale $r$ determined from the cluster correlation data with that determined from the APM survey fixes the value of $\Omega$.
5. The value of $\Omega$ determined in this way turns out $\simeq 0.25$–$0.3$; the same value is implied by the dynamics of the Coma Cluster.
6. If $\Omega = 1$, the amplitude of $\Delta(M)/\Delta_8$ determined from the cluster correlation data does not pass through unity at $8\ h^{-1}$ Mpc.

## 7. GALAXY FORMATION AND HIGH-$z$ OBJECTS: CONSTRAINING THE SMALL-SCALE PREGALACTIC DENSITY FIELD

In the previous sections we discussed constraints on the spectrum of the pregalactic density field from present-day data. The smallest scales on which such constraints allow us to probe the pregalactic density field come from the cluster correlation amplitude–richness dependence and are around $5\ h^{-1}$ Mpc (cf. Fig. 13). On smaller scales, the spectrum of the pregalactic density field is constrained by observations of collapsed objects at high $z$ (Cavalieri & Szalay 1986; Efstathiou & Rees 1988, hereafter ER88; Kashlinsky & Jones 1991; Kashlinsky 1993, hereafter K93). Since the amplitude of the power spectrum is fixed by the requirement that at $z = 0$ it should reproduce unity fluctuation in galaxy counts over a sphere of radius $r_8$, then for a given spectrum this normalization determines at what $z$ the first objects of a given mass scale would typically collapse. For example, in the CDM models (eq. [2]), any increase in the amount of power on large scales would come at the expense of the power on small scales. Consequently, observations of collapsed objects at high redshifts when used in conjunction with the large-scale structure data can set strong constraints on CDM models (K93). In this section we discuss what the latest observational data imply. We also discuss the way the properties of the present-day (elliptical) galaxies constrain the density fluctuations from which they grew and collapsed.

The data at high $z$ that we use come from observations of three types of objects at high redshifts: QSOs, galaxies, and clusters of galaxies. We discuss below the latest data on each of these.

The latest grism surveys have been successful in finding quasars out to $z \simeq 5$ (e.g., Schneider et al. 1992, 1994). There are now a couple of dozen quasars with $z > 4$ (e.g., Turner 1991 and references therein). This highest redshit comes from an optically selected quasar with $z \simeq 4.9$ (Schneider, Schmidt, & Gunn 1991). There are suggestions that the true QSO abundance at high redshift may be significantly higher with most quasars hidden by dust obscuration (Fall & Pei 1993). On the other hand, analysis of the grism surveys shows that the QSO comoving density peaks at $z \sim 2$–$3$ and drops by a factor $\sim 5$ by redshift $\simeq 4.5$ (Schmidt, Schneider, & Gunn 1991). This is also confirmed by data from the radio-loud quasars, which are less likely to be affected by dust (Shaver et al. 1996). Attempts have been made to use the QSO comoving density data at high $z$ to test cosmological models (ER88; K93; Mahonen, Hara, & Miyoshi 1995). In order to do this, one has to derive the total collapsed masses associated with high-redshift quasars, and if, as is commonly assumed, QSOs hide an underlying galaxy, one has to assume further the efficiency with which galactic central nuclei lead to QSO phenomena (e.g., Begelman & Rees 1978; ER88). The lower bound on the mass comes from the Eddington luminosity limit on the total quasar power, and the upper limit on the efficiency is less than 1. If one assumes that a galaxy is hidden behind each quasar, the total mass that collapsed at its redshift would be greater than $10^{12}\ M_\odot$; the same number would be required by reasonable energy conversion efficiencies

associated with the central engines (ER88; Turner 1991). In this case, low-Ω CDM models would be the most difficult to reconcile with the QSO abundance at $z \simeq 4.5$–5, atlhough Haenhelt & Rees (1993) argue that the required factors may be brought into agreement with CDM requirements at high $z$. While quasars can provide useful diagnostics of the various models, the uncertainties in their total mass, number densities, and the redshift of their collapse, rather than the redshift at which they are observed, make such constraints somewhat model dependent.

Clusters of galaxies subtend linear scales comparable to $r_8$, where the rms density contrast today is unity. Therefore, the existence of collapsed clusters of galaxies at high redshifts would imply a large initial density contrast on scale comparable to $r_8$ and would be difficult to reproduce in models with $\Omega = 1$ (K93). The data on the existence of clusters of galaxies at high $z$ is only now becoming available, but it already indicates that galaxies may have assembled into clusters as rich as Coma somewhere before $z \sim 1$–2. Pascarelle et al. (1996) reported a serendipitous discovery of a cluster or group of galaxies at $z \simeq 2.4$ in the Hubble deep field. Francis et al. (1996) report the discovery of a group of red, and therefore old, galaxies at roughly the same redshift. LeFevre et al. (1996) discovered a cluster (or possibly group) of galaxies at $z \simeq 3.14$. Dickinson (1993) reported observations indicating the presence of righ galaxy clusters with a population of extremely red galaxies at $z = 1.2$. Recently, Jones et al. (1997) detected a decrement in the temperature of the microwave background of 560 $\mu$K toward a pair of quasars at $z \simeq 3.8$. Assuming this to be due to the Sunyaev-Zeldovich effect, they searched for a cluster of galaxies in that direction and concluded that the cluster must be at $z > 1$ with the total mass of $\sim 10^{15}\ M_\odot$ (Saunders et al. 1997). Furthermore, such cluster mass and redshift are consistent with the quasar pair, observed to have very similar spectra and separated by $\simeq 10''$, being gravitationally lensed images of the same quasar. Deltorn et al. (1997) identified what is probably a massive cluster ($\sim 10^{15}\ M_\odot$) at $z \simeq 1$ around a high-redshift galaxy 3CR 184 at the same redshift. The cluster is identified through both the gravitational arc near the central galaxy and the excess of galaxies in the redshift distribution around 3CR 184. All this suggests that clusters of galaxies may already have formed at $z \gg 1$. Implications of the existence of such massive clusters at high redshifts for CDM models were discussed in K93. Figure 2*c* in K93 shows that such massive objects must be extremely rare fluctuations, greater than 7–10 standard deviations, in the density field of the CDM models. Most easily they could be explained by assuming low Ω *and* the pregalactic density field having power in excess of the CDM models at these scales.

Galaxies at high redshifts are, probably, the most useful tool in constraining the power spectrum, because in this case (at least) stellar mass can be fairly reliably estimated from colors and stellar populations. Until recently, only a handful of galaxies, all of them steep-spectrum radio sources, have been found at high $z$, the most distant of which were 0902+34 and 4C 41.17 at redshifts of 3.4 and 3.8, respectively (Chambers et al. 1990; Lilly 1988). Chambers & Charlot (1990) modeled their $K$-band photometry from Lilly (1988) with a rapid burst of star formation and concluded that the redshifts of formation must have been greater than 4. Eisenhardt & Dickinson (1992) have reobserved the 0902+34 galaxy at $z = 3.8$ in the $K$-band and argue for its younger age. Eales et al. (1993) have discovered an optically luminous and massive radio galaxy 6C 1232+39 at $z = 3.22$. Lacy et al. (1994) found a radio galaxy 8C 1435+635 with a record $z = 4.25$. Djorgovski et al. (1996) report the discovery of a galaxy responsible for a high-redshift damped Ly$\alpha$ system at $z = 3.15$; from the velocity field, they estimate the dynamical mass of the galaxy at greater than $2 \times 10^{11}\ h^{-1}\ M_\odot$ within $15\ h^{-1}$ kpc. Hubble Deep Field observations of Steidel et al. (1996) and Giavalisco et al. (1996) find populations of normal star-forming galaxies at $z > 3$. Lowenthal et al. (1997) have followed with spectroscopic observations at Keck of the Hubble Deep Field galaxies and, with the sixteen confirmed sources, concluded that the comoving density of $z > 3$ galaxies is greater than $2 \times 10^{-3}\ h^3$ Mpc$^{-3}$ if $\Omega = 0.1$ or greater than $10^{-2}\ h^3$ Mpc$^{-2}$ if $\Omega = 1$. For comparison, the comoving density of $L_*$ galaxies today is $\Phi_* \simeq 1.4 \times 10^{-2}\ h^3$ Mpc (Loveday et al. 1992). Trager et al. (1997), using the Keck Telescope, discovered four high-redshift galaxies: one at $z = 3.35$ and three at $z \simeq 4$. Using the Ly$\alpha$ break as redshift indicator, Hu & McMahon (1996) reported the possible discovery of star-forming Ly$\alpha$-emitting galaxies at $z = 4.55$. The above data indicate that galaxies must have present already at $z \sim 5$. In an exciting recent discovery Franx et al. (1997) identified a gravitationally lensed arc as a galaxy at $z = 4.92$ and further find a companion to it with a radial velocity of only 450 km s$^{-1}$. Thus the data show that galaxies must already have been present in the universe at redshifts beyond $\sim 5$. The existence of such early formation (collapse) of objects on scales $\sim 10^{12}\ M_\odot$ is indicative of small-scale power in the pregalactic density field in excess of that given by the low-Ω CDM models required by the APM data (K93).

Further indications of when galaxies must have collapsed come from recent observations of galaxies at smaller redshifts, but for which detailed spectroscopy and therefore accurate age determination are available. Hu & Ridgway (1994) found galaxy candidates whose colors were consistent with colors of ellipticals with old stellar populations shifted to $z \sim 2.5$ and have provided the first evidence that galaxies at high redshifts may already contain old stellar populations. A real breakthrough came with observations of the 53W091 galaxy at $z = 1.55$ by Dunlop et al. (1996, hereafter D96). D96 obtained high-resolution spectroscopy of 53W091 with the Keck Telescope that revealed a very old stellar population in the galaxy. By fitting the spectrum with stellar models, they determined its age to be $t_{53W091} = 3.5$ Gyr with a very small dispersion (0.5 Gyr at the 90% confidence level). This would rule out an Einstein–de Sitter universe for any $H_0 > 40$ km s$^{-1}$ Mpc$^{-1}$ and, for open or Λ-dominated flat models, would place formation of 53W091 at high redshifts $z > 4$–5. That this galaxy is unlikely to be either unique or unusual is evidenced by discovery of more such objects—53W069 at $z = 1.41$ with age $t_{53W069} = 4$ Gyr and 0.5 Gyr uncertainty (Dey et al. 1997). Francis, Woodgate, & Danks (1977) report discovering two high-redshift galaxies at $z = 2.38$ with an old stellar population greater than 0.5 Gyr.

Kashlinsky & Jimenez (1997), hereafter KJ97, discussed implications of the 53W091 data on low-Ω flat ($\Omega + \lambda = 1$, where $\lambda = \Lambda/3H_0^2$) CDM models. They pointed out that the redshift of formation of 53W091 required by its age would decrease with decreasing Ω. But at the same time, decreasing Ω would in such models suppress the power on small scales, thereby delaying galaxy collapse. KJ97 computed the total stellar mass of 53W091 by fitting the observed flux in all ($V$, $J$, $H$, $K$) bands with synthetic galaxy spectra based on the Miller-Scalo initial mass function for stars. The total mass in stars alone is given in

Table 1 of KJ97 and is $\geq 10^{12} M_{\odot}$ inside the aperture radius subtending (8–15) $h^{-1}$ kpc at $z = 1.55$. The resultant stellar mass has little dependence on cosmological parameters or metallicity. KJ97 showed that in the flat $\Lambda$-dominated CDM cosmogonies, 53W091 would have to be greater than $\simeq 5$ standard deviations in the pregalactic density field.

Further observational constraints on $\Omega + \lambda = 1$ cosmologies come from the data on high-redshift Type Ia supernovae. The latest measurements include seven Type Ia supernovae out to $z \simeq 0.46$ and set limits of $\lambda < 0.35$ at the 68% or $\lambda < 0.51$ at the 95% confidence level (Perlmutter et al. 1997). Similarly, the data on gravitational lenses implies $\lambda < 0.66$ at the 95% confidence level (Kochanek 1996). Together with the KJ97 results, this makes flat $\Lambda$-dominated cosmogonies less attractive than open universe cosmogonies. Therefore, in the remainder of this section we evaluate the limits on the pregalactic density field assuming $\Lambda = 0$, but most of the results can be relatively easily extended to $\Lambda \neq 0$. For an $\Omega + \lambda = 1$ universe, our main conclusions will not differ appreciably from the open universe case.

As discussed above, the epoch of galaxy collapse constrains the pregalactic power spectrum on galaxy scales, and the data on the 53W091 galaxy place strong constraints on $\Lambda$-dominated flat universe CDM models. In what follows, we generalize the discussion of KJ97 to open universe. Figure 14 plots the redshift of formation of the stellar population of 53W091 versus $\Omega$. Dotted lines correspond to the best estimate of its age from D96, $t_{53W01} = 3.5$ Gyr. Solid and dashed lines correspond to $\pm 0.5$ Gyr uncertainty in $t_{53W01}$ at 95% confidence level. Three lines of each type correspond to the Hubble constant values of $h = 0.5$, 0.6, and 0.75. The age of 53W091 implies large values of the redshift of its formation, $z_{for} \geq 5$, and agrees well with observations of other high-redshift galaxies discussed earlier in this section. The numbers for another galaxy, 53W069 (Dey et al. 1997), would be similar, and neither galaxy is consistent with the $\Omega = 1$ universe for any reasonable values of the Hubbble constant ($h > 0.4$).

In order to estimate the likelihood of formation of objects like 53W091 in open CDM models, we proceed in the manner outlined in K93. We start with the density field in the linear regime at some early epoch $z_i$; in the formalism outlined in K93 and KJ97 the final results are independent of $z_i$. We denote by $\delta_{col}$ the amplitude the density fluctuation had to have at $z_i$ in order to collapse at redshift $z$. It can be evaluated from the spherical model approximation (e.g., Peebles 1980; Gott & Rees 1975; Narayan & White 1988; K93). The time evolution of a spherical shell that contained density contrast $\delta_i$ at $z_i$ can be described by its "Friedmann" equation: $\dot{r}^2 = A/r + C$, where $A = H_0^2 \Omega$ and $-C = H_0^2[\frac{5}{3}\Omega\delta_i(1 + z_i) + \Omega - 1]$ and $r$ is the expansion factor of the fluctuation. The turnaround time is given by $t(\dot{r} = 0) = (\pi/2)A(-C)^{3/2}$, and the collapse time is $t_{col} = 2t_{ta}$. The value of $\delta_{col}$ is then determined by the condition that $t_{col}$ equals the cosmic time that elapsed between $z_i$ and the redshift $z$ when the fluctuation collapses:

$$\frac{\pi}{H_0} \frac{\Omega}{(5/3\Omega\delta_{col} z_i + \Omega - 1)^{3/2}} = \int_z^{z_i} \frac{dz}{(1+z)^2\sqrt{1+\Omega z}} . \tag{34}$$

In order to normalize the density field at $z_i$ and also eliminate the dependence on $z_i$, we compute also the amplitude, $\Delta_{8,i}$, which the fluctuation had to have at $z_i$ in order to grow to $1/b$ amplitude at $z = 0$. This can be done by noticing that conservation of mass requires $1 + \delta(z) = (1 + \delta_i)[r_i/r(z)]^3$. The fluctuation starts with $\Delta_{8,i}$ and must reach a density contrast of $1/b$ at $z = 0$. The time it takes is $\int_{r_i}^{r(z=0)} dt/\dot{r}$ with $r(z = 0)$ and $r_i$ related by the above mass conservation expression. Hence the equation for $\Delta_{8,i}$ is given by

$$\int_{(1-\Delta_{8,i}/3)/(1+z_i)}^{(1+1/b)^{-1/3}} \frac{dr}{\sqrt{\Omega r^{-1} + 1 - \Omega - (5/3)\Omega\Delta_{8,i} z_i}} = \int_0^{z_i} \frac{dz}{(1+z)^2\sqrt{1+\Omega z}} . \tag{35}$$

For $z_i \gg 1$ and $\delta_{col}, \Delta_{8,i} \ll 1$, the ratio $\delta_{col}/\Delta_{8,i}$ determined from equations (34) and (35) is independent of $z_i$. We are interested in the pregalactic spectrum of density fluctuations and in linear regime fluctuations evolve independently of $z$. Hence, in what follows we omit the subscript $i$ in the ratios $\delta/\Delta_8$ as long as both amplitudes correspond to the pregalactic density field.

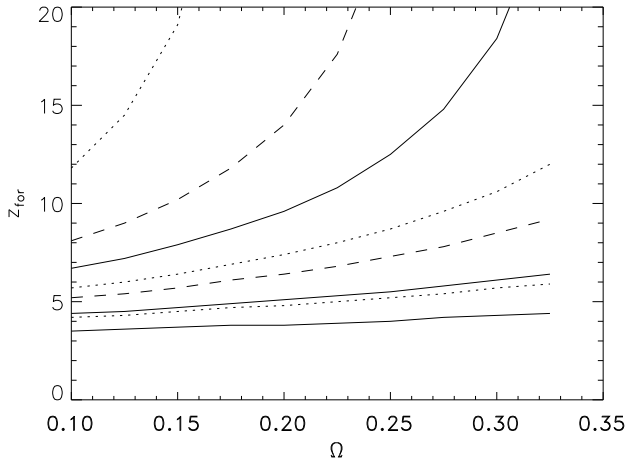


FIG. 14.—Redshift of formation of 53W091 according to the age estimate $t_{age} = 3.5 \pm 0.5$ Gyr of D96 plotted vs. $\Omega$ for $\Lambda = 0$. Dotted lines correspond to $t_{age} = 3.5$ Gyr, solid lines to $t_{age} = 3$ Gyr, and dashed lines to $t_{age} = 4$ Gyr. Three lines of each type correspond to $h = 0.5$, 0.6, and 0.75, from botton up.

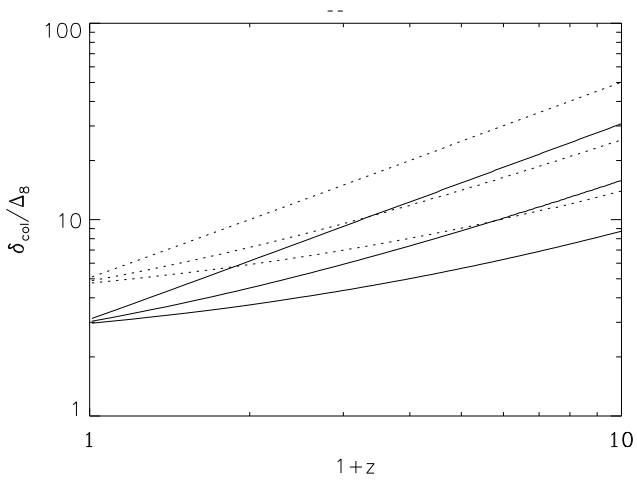


FIG. 15.—Values of $\delta_{col}/\Delta_8$ at an early epoch, $z_i$, plotted vs. redshift of collapse $z$ plotted for $\Lambda = 0$. Solid lines correspond to $\Delta_8$ evolving to 1 today, or $b = 1$, and dotted lines are for $b = 2$. Three lines of each type correspond to $\Omega = 1$, 0.3, and 0.1, from top down.

Figure 15 plots $\delta_{col}/\Delta_8$ versus $1 + z$ at which the fluctuation collapses for $\Lambda = 0$. Solid lines correspond to $b = 1$ and dotted lines to $b = 2$, but the solution of equation (35) scales according to $\Delta_{8,i} \propto b^{2/3}$. The three lines of each type correspond to $\Omega = 0.1$, 0.3, and 1, from bottom to top. One can see that the growth of density fluctuations slows down after $1 + z \simeq \Omega^{-1}$. Figure 15 in conjunction with $z_{for}$ shown in Figure 14 allows one to estimate the density field of 53W091 and the likelihood of its formation in a given cosmological model given the total mass of the galaxy. (For $\Omega + \lambda = 1$, the ratio $\delta_{col}/\Delta_8$ is plotted in Figure 1*c* of K93; in that case, the growth of fluctuations freezes at $1 + z \simeq \Omega^{-1/3}$.)

KJ97 estimated that the stellar mass of 53W091 must be at least $10^{12}\ M_\odot$ with little dependence on cosmology or star formation history. Thus, in order to estimate the likelihood of 53W091 in the open CDM models, we adopt a (conservative) value for its *total* mass of $5 \times 10^{12}\ M_\odot$. Figure 16 illustrates the likelihood of 53W091 forming in the open CDM models. Thick lines in Figure 16 show the value of the rms fluctuation, $\Delta(M)$, in units of $\Delta_8$ in the open CDM models on the (total) mass scale of $5 \times 10^{12}\ M_\odot$. At this mass range the CDM spectra have an effective power slope index of $\simeq -2.5$, so the ratio $\Delta(M)/\Delta_8$ is proportional to $M^{-0.1}$ over the mass scales relevant for 53W091. The three lines from top to bottom correspond to $H_0 = 75$, 60, and 50 km s$^{-1}$ Mpc$^{-1}$. Thin lines show the bias-factor–independent values of $\delta_{53W091}/(\Delta_8 b^{2/3})$ evaluated from equations (34) and (35) at the redshift plotted in Figure 14. Notation of the thin lines in Figure 16 is the same as in Figure 14. The values of the bias parameter for such models are determined by normalization to the *COBE* DMR data and are $b > 1$ (e.g., Stompor et al. 1995). One can see from the figure that similarly to the flat, $\Omega + \lambda = 1$, CDM models discussed in KJ97, the data on 53W091 would require it to be a very rare (greater than 5 standard deviations) fluctuation in the density field of open CDM models.

While the above arguments allow one to rule out or confirm certain cosmological models, they show only how rare the observed object is in a given model and thus do not allow us to estimate the amount of power in the small-scale pregalactic density field directly. Furthermore, estimating the number density of such objects requires assumptions about the "Gaussianity" of the pregalactic density field. For example, at a given number of standard deviations, for Gaussian models such as CDM, collapsed objects would be less abundant than in models with a non-Gaussian density field, such as strings (cf.

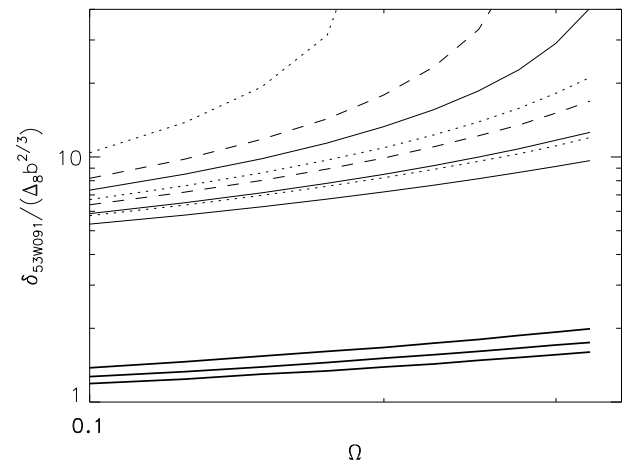


FIG. 16.—Values of $\delta_{col}/\Delta_8$ implied by the redshift of collapse of 53W091 in Fig. 14 plotted vs. $\Omega$ for a zero cosmological constant universe. Three thick solid lines show the predictions of this ratio in CDM models with the value of $\Omega$ shown on the horizontal axis. The total mass of 53W091 there was taken to be $5 \times 10^{12}\ M_\odot$ (cf. KJ97). The three thick lines correspond to $h = 0.5$, 0.6, and 0.75, from bottom up.

Mahonen et al. 1995). A different argument about galaxy formation epoch is required in order to estimate the small-scale pregalactic density field directly.

We now move to estimating the epoch of galaxy formation from the *present day* galaxies and then estimating directly the density field from which they formed. We assume that galactic halos formed by dissipationless gravitational clustering (cf. White & Rees 1978). We assume further that the forming halo turns around at radius $r_{ta}$ with little kinetic energy, i.e., its total energy per unit mass is $E = -GM/r_{ta}$. The ensuing cold collapse will lead to violent relaxation during which the time-dependent gravitational potential redistributes energy and particle distribution (Lynden-Bell 1967), while the total mass of the halo remains conserved. Thus, at the end of the violent relaxation, the kinetic energy $T$ and potential energy $V$ will be related by the virial equilibrium relation: $2T + V = 0$, *i.e.*, the total energy per unit mass is $E = T + V = -T = -(3/2)\sigma^2$, where $\sigma$ is the one-dimensional halo velocity dispersion after virialization. From the above the latter would be given by $\sigma^2 = (2/3)GM/r_{ta}$. We now assume that the halo turns around at redshift $z_{ta}$ with an overdensity $\gamma_{ta}(z_{ta})$ with respect to the average density of the universe, $(3H_0^2/8\pi G)\Omega(1 + z_{ta})^3$, at that epoch. Therefore, for halo that has one-dimensional velocity dispersion $\sigma$ and, at least initially, had total mass $M$ (which later could have been lost by tidal stripping, for example), the redshift of its turnaround is given by

$$\sigma^2 = \frac{2^{2/3}}{3}(GMH_0)^{2/3}[\Omega\gamma_{ta}(z_{ta})]^{1/3}(1 + z_{ta}) , \tag{36}$$

or in terms of numbers,

$$\Omega^{1/3}[\gamma_{ta}(z_{ta})]^{1/3}(1 + z_{ta}) = 13.3\left(\frac{\sigma}{200 \text{ km s}^{-1}}\right)^2\left(\frac{M}{10^{12}\ h^{-1}\ M_\odot}\right)^{-2/3} . \tag{37}$$

Once the redshift of the halo turnaround has been evaluated, one can calculate the redshift of its collapse, $z_{col}$, by assuming the collapse to have taken twice the turnaround time (e.g., Gott & Rees 1975). As expected, at a given $\sigma$ the low-mass halos should have collapsed at higher redshifts.

We turn to computing the turnaround overdensity $\gamma_{ta}(z) = \rho_{ta}/\bar{\rho}(z_{ta})$. The turnaround time of a fluctuation is given by

$$t_{ta} = t(\dot{r} = 0) = \frac{\pi}{2H_0}\frac{\Omega}{[(5/3)\Omega\delta_i z_i + \Omega - 1]^{3/2}} .$$

On the other hand, the linear scale at the turnaround is $r_{ta} = r_i\Omega/[(5/3)\Omega\delta_i z_i + \Omega - 1]$, so the mean fluctuation density at the turnaround is given by

$$\rho_{ta} = \frac{3H_0^2}{8\pi G}\frac{[(5/3)\Omega\delta_i z_i + \Omega - 1]^3}{\Omega^2} .$$

Rewriting the right-hand side of the above expression in terms of cosmic time at turnaround, $t_{ta}$, leads to

$$\gamma_{ta}(z) = \frac{\rho_{ta}}{\bar{\rho}(z)} = \left(\frac{\pi}{2}\right)^2\frac{1}{\Omega(1 + z)^3[H_0\, t(z; \Omega)]^2} . \tag{38}$$

For $\Omega = 1$, one recovers from equation (38) a well-known result of $\gamma_{ta}(z) = (3\pi/4)^2$. For low values of $\Omega$, the density contrast at turnaround is larger. Figure 17 plots $\gamma_{ta}$ versus $z$ for $\Omega = 0.1$ (*dashed lines*), 0.3 (*dotted lines*), and 1 (*solid line*). At $1 + z > \Omega^{-1}$, the values of $\gamma_{ta}$ converge to $(3\pi/4)^2$.

Equations (37) and (38) allow one to estimate the redshift of galaxy collapse, given by $t_{col} = 2t_{ta}$, for the halo of one-dimensional velocity dispersion $\sigma$ and mass $M$. Figure 18 plots the value of $z_{col}$ versus $\Omega$ for a galaxy with $\sigma = 200$ km s$^{-1}$.

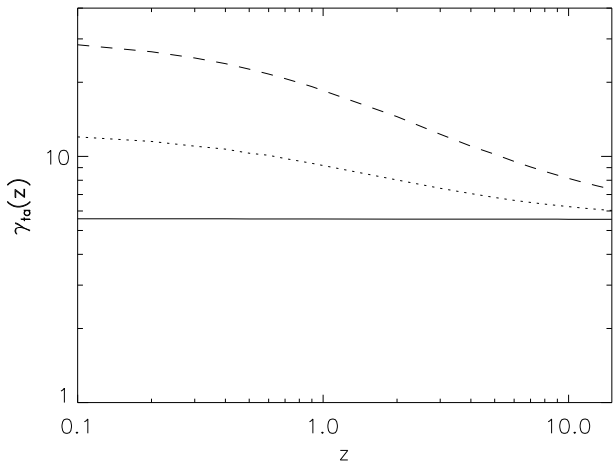


FIG. 17.—Overdensity of the fluctuation at turnaround plotted vs. the turnaround redshift. Solid line is for $\Omega = 1$, dotted line for $\Omega = 0.33$, and dashed line for $\Omega = 0.1$.

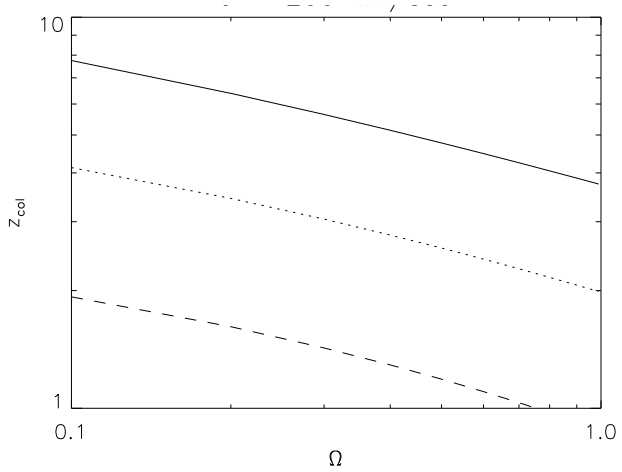


FIG. 18.—Redshift of collapse (formation) of galaxy with the halo dispersion $\sigma = 200$ km s$^{-1}$ vs. Ω, according to eq. (37). The total (initial halo) mass is taken to be $10^{12}\,h^{-1}\,M_\odot$ (*solid line*), $2 \times 10^{12}\,h^{-1}\,M_\odot$ (*dotted line*), and $4 \times 10^{12}\,h^{-1}\,M_\odot$ (*dashed line*).

The solid line corresponds to $M = 10^{12}\ h^{-1}\ M_\odot$, the dotted line to $M = 2 \times 10^{12}\ h^{-1}\ M_\odot$, and the dashed line to $M = 4 \times 10^{12}\ h^{-1}\ M_\odot$. If Ω is low, the redshifts at which such a galaxy should have formed are in general agreement with the data discussed in this section. If however, $\Omega = 1$, then massive galaxies would form at redshifts lower than observations indicate.

In fact, one can narrow down the range of $z_{col}$ if one uses the observed properties of galaxies in order to compute the total halo mass and its velocity dispersion. In order to estimate the total halo mass at the time of its formation, we proceed as follows. Encouraged by the results that normalization to the observed properties of Coma gave in the previous section, we assume that this cluster is representative of the global value of the mass-to-light ratios associated with galactic systems. In order to relate the initial mass of the halo to the luminosity of the galaxy it contains, we use the $D_n$-$\sigma$ relation for elliptical galaxies (Dressler et al. 1987a; Djorgovski & Davis 1987). In obtaining our results, we will thus be restricted to elliptical galaxies, but we will assume that the results are representative of the entire galaxy population. The fundamental-plane relations of ellipticals are equivalent to the mass-to-light ratio of stellar populations of ellipticals scaling $\propto L_B^{\kappa}$. From a detailed study of 37 ellipticals by van der Marel (1991) we adopt $\kappa = 0.35$. Assuming further that the ratio of the dark to luminous matter is constant throughout the universe and that luminous parts of galaxies formed by gas dissipation inside formed halos (White & Rees 1978) would allow to relate the total (initial) mass of formed halos to the blue luminosity of the present-day galaxies. (By "initial" we mean the mass at the time of the halo collapse; clustering processes would later have stripped parts, or all, of the halo material to form a continuous dark matter distribution of clusters and groups of galaxies.) Thus, the mass of the halo at the time of its collapse is assumed to be given by

$$M_{\rm halo} = \left(\frac{M}{L_B}\right)_{\rm Coma} \frac{\Gamma(2-\alpha)}{\Gamma(2+\kappa-\alpha)} \left(\frac{L_B}{L_*}\right)^{1+\kappa} \simeq 1.1 \left(\frac{M}{L_B}\right)_{\rm Coma} \left(\frac{L_B}{L_*}\right)^{1.35} . \tag{39}$$

The Γ-function factors in equation (39) come from requiring that $(M/L)_{\rm Coma} = \int \Phi(L) M(L) dL / \int \Phi(L) L\, dL$ with $\Phi(L) = L_*^{-1} \Phi_* (L/L_*)^{-\alpha} \exp(-L/L_*)$.

Observationally it is known that inner parts of elliptical galaxies are dominated by both stellar and halo potentials (e.g., Rix et al. 1997), which would be consistent with ellipticals forming by dissipational collapse (Kashlinsky 1982). Thus, central velocity dispersions of elliptical galaxies would not provide a good measurement of the halo potential well. The latter can be determined from dynamics in the outer parts of elliptical galaxies, where the only available measurements today come from X-ray data from hot gas coronae. The best measurements of temperature electron density profiles around ellipticals come from the *ASCA* (Matsumoto et al. 1997; Matsushita 1997) and *ROSAT* (Davis & White 1996) satellites. Since the cooling time of the gas is of the order of $H_0^{-1}$, the gas is likely to be hydrostatic. Then its temperature will be related to the halo velocity dispersion via the equation of hydrostatic equilibrium, which for an isothermal halo profile reads, $d(k_{\rm B}\, n_{\rm gas}\, T)/dr = -\mu m_p\, \sigma^2/r$, where $k_{\rm B}$ is the Boltzmann constant, $\mu$ is the molecular weight, and $m_p$ is the proton mass (e.g., Awaki et al. 1994). Temperature profiles (Matsushita 1997) indicate that the gas in outer parts can be assumed to be isothermal and that the gas has a density profile $n_{\rm gas} \propto r^{-\beta_{\rm gas}}$ with $\beta_{\rm gas} \simeq 2.5$–3. Then the halo velocity dispersion is related to the measured X-ray temperature via

$$\sigma = \left(\frac{k_{\rm B}\, T}{\mu \beta_{\rm gas}\, m_p}\right)^{1/2} . \tag{40}$$

Equations (37)–(40) along with the numbers in Figure 15 now allow us to determine the density fluctuation spectrum given photometric ($L_B$) and X-ray ($T$) data on galaxies.

We have computed the values of $\delta(M)/\Delta_8$ using equations (37)–(40) for a sample of galaxies for which good X-ray and photometric data are available. The halo velocity dispersion was computed according to equation (40) from the *ROSAT* (Davis & White 1996) and *ASCA* (Matsumoto et al. 1997) observations. The data on the blue absolute luminosities were taken from Faber et al. (1989), who determined the absolute luminosities using the fundamental-plane relations. Only galaxies that

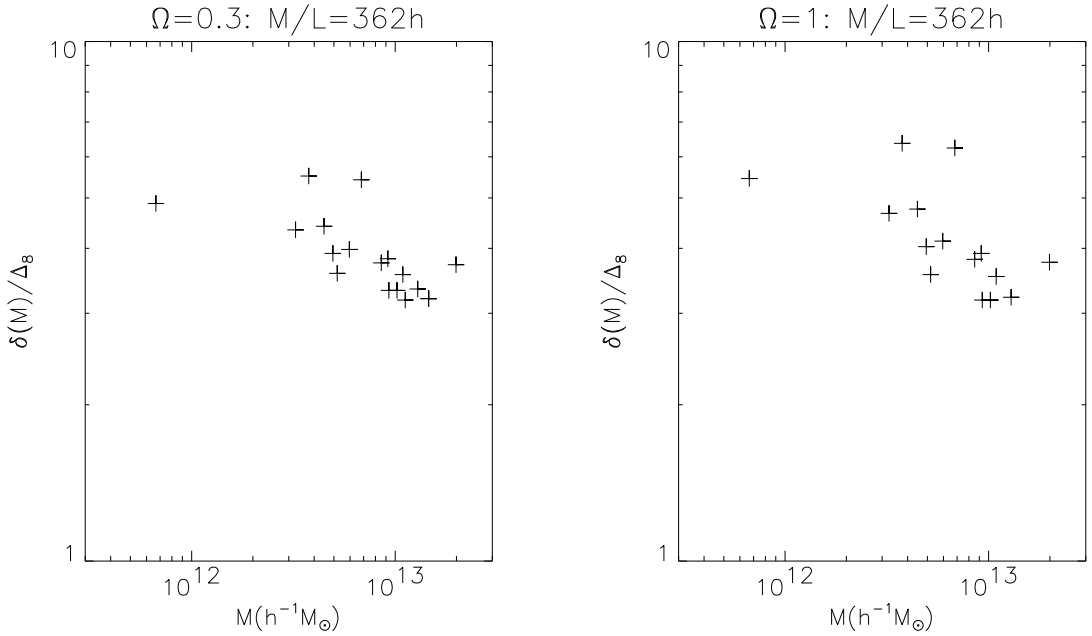


FIG. 19.—Density fluctuations $\delta(M)/\Delta_8$ computed according to eqs. (37)–(40) vs. the mass scale they contain. The numbers were computed normalizing the total mass-to-light ratio of galaxies to Coma at $M/L = 362\ h$. The left-hand panel assumes $\Omega = 0.3$, corresponding to the value implied by Coma dynamics, and the right-hand panel corresponds to $\Omega = 1$.

appear in both the X-ray and Faber et al. (1989) catalogs were used. The *ROSAT*-determined X-ray temperatures and gas profiles for galaxies have larger uncertainties than those of *ASCA*; hence, of the *ROSAT* data listed in Table 1 of Davis & White (1996), we kept only the data for those galaxies that have quoted uncertainties in $T$ of less than 25%. The *ASCA* data available are listed in Table 3 of Matsumoto et al. (1997). Note that the atomic modeling of the spectra alone can introduce *systematic* uncertainties of $\sim 20\%$ (Matsushita 1997). The final data set for which we found the accurate X-ray temperature measurements and photometry included some twenty galaxies.

Figure 19 plots the values of $\delta(M)/\Delta_8$ versus the initial halo mass computed from equations (37)–(40) assuming a "universal" hot gas profile of $\beta_{\rm gas} = 2.5$ and $\mu = 0.6$; the numbers in equation (40) are not very sensitive to the value of $\beta$ observed to lie between 2 and 3. The left-hand panel shows the results for $\Omega = 0.3$, as required by the Coma Cluster dynamics. The right-hand panel assumes the initial dark halos to have the total mass-to-light ratio like that of Coma, but the total $\Omega$ to be 1. Note that this prescription gives the actual amplitude of the density fluctuation rather than its rms value $\Delta(M)$, and hence should have larger scatter. Additional scatter in Figure 19 is introduced by the uncertainties in the current X-ray data and modeling and a further $\simeq 15\%$ uncertainty in the individual distances from using the fundamental-plane relations. The slope in Figure 19 is quite obvious and is in good agreement with the slope determined for large scales. The scatter is larger, though, but is expected given the above observational uncertainties, the simplifying assumptions that were used in this section, and the fact that the actual $\delta(M)$ rather than the rms, $\Delta(M)$, is shown. On the other hand, the X-ray temperatures do not correlate with the central velocity dispersion, and so the Faber-Jackson blue luminosity–central velocity dispersion correlation is unlikely to reproduce the trend in Figure 19. It is likely that the numbers in Figure 19 reflect the slope and amplitude of the pregalactic density field on the corresponding mass scales.

## 8. RECONSTRUCTED DENSITY FIELD AND COSMOLOGICAL PARADIGMS

The methods outlined in §§ 3–7 allowed us to reconstruct pregalactic density field from various astronomical data on scales from $\sim 1$ to $100\ h^{-1}$ Mpc. Figure 20 summarizes the results in terms of the quantity

$$\frac{\Delta(M)}{\Delta_8} = \left[\frac{\int_0^\infty P(k) W_{\rm TH}(kr) k^2\, dk}{\int_0^\infty P(k) W_{\rm TH}(kr_8) k^2\, dk}\right]^{1/2}, \tag{41}$$

with $r$ being the linear scale containing mass $M$ according to equation (32). The left-hand panel corresponds to $\Omega = 0.25$, the value suggested by the dynamics of the Coma Cluster and galaxy luminosity function. The right-hand panel plots the reconstructed field for $\Omega = 1$, implied by inflationary prejudices.

The open square in the figure shows the "normalization" point where the above quantity is unity by definition and irrespective of the bias factor. The three dotted lines show the BE93 fit to the APM data with 1 standard deviation uncertainty, and the three lines correspond to the less accurate, but earlier, K92 fits to the data. The lines are drawn following the peculiar velocities analysis in § 4, suggesting the constancy of the bias parameter, $b$. They are plotted on scales greater than $r_8$, where the APM data are less affected by nonlinear gravitational effects. On scales greater than $100\ h^{-1}$ Mpc the APM data probably are not useful for reliably probing the pregalactic density field. The diamonds show the values for $\Delta(M)/\Delta_8$ reconstructed in §§ 5 and 6 from the data on the cluster correlation amplitude versus richness relation and normalizing the

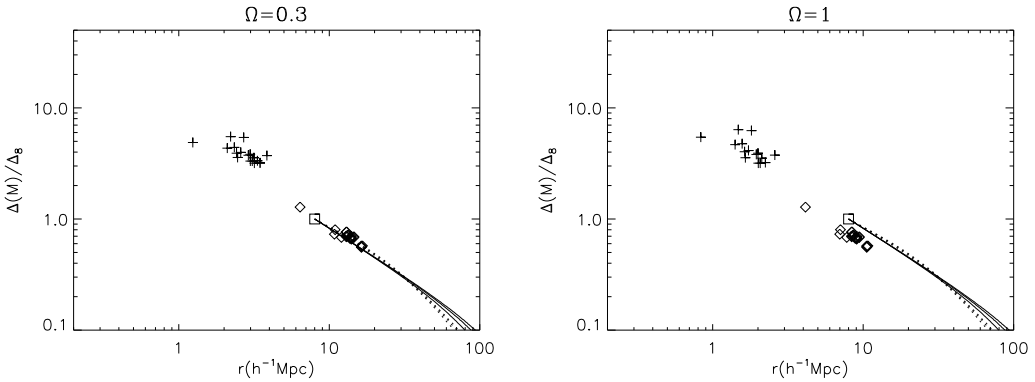


FIG. 20.—Pregalactic density field, $\Delta(M)/\Delta_8$ reconstructed over the entire range of 1 $h^{-1}$ Mpc $< r <$ 100 $h^{-1}$ Mpc. The left-hand panel corresponds to $\Omega = 0.3$, and the right-hand panel corresponds to $\Omega = 1$. The open square corresponds to the value of 1 at $r_8$. The lines from the APM data are plotted only for linear scales $r > r_8$. Solid lines are the K92 fits to the APM data with the transition scale $k_0^{-1} = 35$, 40, and 50 $h^{-1}$, from bottom up. The three dotted lines correspond to the BE93 fit with 1 standard deviation uncertainty. Diamonds show the values obtained from inverting the data on cluster correlation amplitude vs. richness, according to eq. (29). The diamonds coincide with the APM data only if $\Omega \simeq 0.3$. Plus signs show the values reconstructed according to eqs. (37)–(40) from the data on the fundamental plane of galaxies and the *ROSAT* and *ASCA* measurements of the halo velocity dispersion.

cluster richness-mass relation to Coma. This reconstruction allows us to determine the pregalactic density field on scales from $\simeq 5$ to $\simeq 20$ $h^{-1}$ Mpc. The two methods should give the same results where they reconstruct the density field on the same scales. For $\Omega = 0.25$–0.3, the density fields reconstructed from the two independent methods coincide. If $\Omega = 1$, the discrepancy between the two amplitudes is significant, although the slopes coincide. Thus, we conclude that $\Omega \simeq 0.25$–0.3 is in better agreement with the data, and the pregalactic density field on scales 5 $h^{-1}$ Mpc $< r <$ 100 $h^{-1}$ Mpc is likely to be close to that in the left-hand panel of Figure 20.

The plus signs in Figure 20 show the density field reconstructed in § 7 by using the fundamental-plane relations and X-ray data for determining halo velocity dispersion. The total halo masses at the time of their collapse/formation were normalized to reproduce the observed blue mass-to-light ratio of Coma. Plotted is the value of $\delta(M)$, not the rms $\Delta(M)$, in units of $\Delta_8$; the numbers plotted depend on the amplitude of the bias parameter, $\propto b^{2/3}$. Both the slope and the amplitudes of the density field on galactic scales are consistent with extrapolation from the density field reconstructed on larger scales assuming a simple power law for $P(k)$ with the slope of $\sim -1$. The slight excess in the amplitude ($\sim 30\%$) of the plus signs should not be regarded as worrisome, since what is plotted is the actual $\delta(M)$, not its rms value. Furthermore, the galaxies used in the fundamental-plane and X-ray studies are found predominantly in rich clusters and may indeed have formed out of higher peaks of the density field. Also, the X-ray temperatures determined from *ASCA* and *ROSAT* observations for galactic X-ray emission may have systematic errors of $\sim 20\%$ due to uncertainties in the atomic physics involved (R. Mushotzky 1997, private communication). Such systematic errors may be sufficient to bring the amplitudes of the plus signs up by the necessary $\simeq 30\%$. In addition, many of the assumptions used here may be too simplifying, e.g., assuming the same slope for the gas profile, $\beta_{\rm gas}$, or there may be deviations from the isothermal density profile, $\rho_{\rm halo} \propto r^{-2}$, assumed here for all halos. Given these uncertainties, we find that the consistency in the density field plotted in Figure 20 from the various data sets and methods is quite reasonable.

Figure 21 juxtaposes the reconstructed density field with the predictions of the CDM models for the Harrison-Zeldovich (*right-hand panel*) and tilted spectra. Notation of the data points is the same as in Figure 20. Only the data points for $\Omega = 0.3$ (*left-hand panel* in Fig. 20) are shown because of the discrepancy between the cluster correlation data and the APM methods for $\Omega = 1$. CDM models are shown with dashed lines: thick dashed lines correspond to $\Omega h = 0.5$ and thin lines to $\Omega h = 0.2$ for

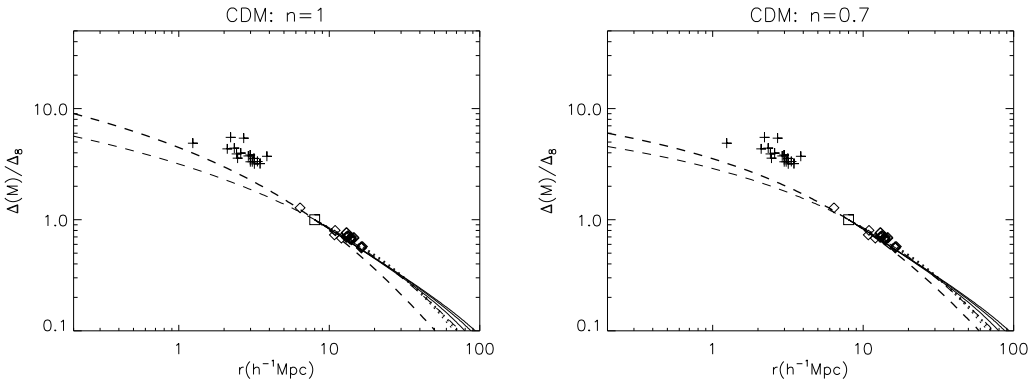


FIG. 21.—Results from the left-hand panel of Fig. 20 juxtaposed with CDM models. In the left-hand panel the dashed lines show the CDM density field with $n = 1$ and $\Omega h = 0.5$ (*thick dashed line*) and $\Omega h = 0.2$. The right-hand panel shows the tilted CDM models with $n = 0.7$ and $\Omega h = 0.5$ (*thick dashed line*) and $\Omega h = 0.3$. Other symbols have the same notation as in Fig. 20.

$n = 1$ and to 0.3 for $n = 0.7$. One can see that the models that fit the large-scale part of the pregalactic spectrum miss the points on small scales by a significant factor. That is, for any value of the excess power, $\Omega h$, or $n$, one would have to assume a significant scale dependence in the bias parameter $b$ in order to fit the density field over the entire range of scales.

The most economical conclusion to draw from the points in Figure 20 would be to assume that (1) the universe is open with $\Omega \simeq 0.25$–0.3, the value which is also suggested by the dynamics of the Coma Cluster, and (2) the pregalactic power spectrum has a constant power index of $\sim -1$ all the way from $\sim 30\ h^{-1}$ Mpc to $\sim 1\ h^{-1}$ Mpc. For primordial adiabatic fluctuations, this could be achieved only if the smaller wavelengths that enter the horizon in the radiation-dominated era have more power when compared with the scale-free primordial spectrum, $P_i(k) \propto k^n$. Computations show that this may be done with strings (Albrecht & Stebbins 1992), although the models are still not definite enough to predict a unique power spectrum. Another possibility could be the primeval baryon isocurvature (PBI) model, where the shape of the spectrum of the density field could be evolving further after recombination due to reionization and other effects (Peebles 1987). One can also assume that the primordial power spectrum in the CDM models was not scale free and contained extra power on small scales. However, the latter may lack theoretical motivation if, as we have argued on the basis of cluster correlation and galaxy data, the universe is open, and CDM model predictions are tied to and/or motivated by an inflationary scenario.

Figure 20 plots the pregalactic density field in units of $\Delta_8$ and thus independently of the latter's value. In order to assign a numerical value to $\Delta(M)$ at some early epoch, e.g., the epoch of recombination, we have to compute the value of $\Delta_8$ at that time. Assuming purely gravitational evolution, i.e., ignoring pressure forces, Thompson drag, and other effects that can become important in some models, would give at $z = 1000$ the values of $\Delta_8 = (0.55, 1.2, 2.8) \times 10^{-3} b^{2/3}$ for $\Omega = (1, 0.3, 0.1)$, respectively. The value of $b$ can be determined from normalization to the microwave background anisotropy measurements. We omit this, since it would require assumptions about the nature of the density field, dark matter, reionization history, etc.

## 9. CONCLUSIONS

The results of the paper can be summarized as follows:

1. Our analysis of the APM survey results on $w(\theta)$ in six 0.5 mag wide slices shows that the various evolutionary corrections are not significant out to the limits of the catalog at $b_J \simeq 20.5$. This allows us to make accurate fits of the various spectra to the APM data. Of these, the BE93 fit for the power spectrum of the density field traced by galaxies gives the best approximation to all six slices. If light traces mass, this fixes the pregalactic density field on scales $10\ h^{-1}$ Mpc $< r < 100\ h^{-1}$ Mpc. We then choose the value of the angular scale at which the angular correlation function is $\simeq 3.3$ times the systematic error from the plate gradients in all six slices to test the requirements the data set on CDM models. We find that in order to fit the APM data, CDM models would require $\Omega h \simeq 0.2$ if $n = 1$ or $\Omega h \simeq 0.3$ if $n = 0.7$.

2. The velocity field implied by the galaxy correlation function determined from the APM data is consistent with the Great Attractor peculiar velocities and the bias parameter, which is constant over the range of scales probed by both data sets, $10\ h^{-1}$ Mpc $< r < 60\ h^{-1}$ Mpc. This suggests that the pregalactic density field is proportional to the power spectrum of galaxy clustering determined from the APM on scales greater than $r_8$. Furthermore, if $\Omega^{0.6}/b = 1$, the amplitude of the dot velocity correlation function at zero lag would be significantly larger, $\simeq (1300\ \mathrm{km\ s^{-1}})^2$, than the values indicated locally and by the central velocity dispersions of typical galaxy systems. This suggests that the velocity data are in agreement with an open universe. Furthermore, we show that the quantity constructed from the velocity correlation tensor, $[\Sigma(r) - \Pi(r)]^{1/2}$, can be used to determine $\Omega^{0.6}/b$. Its amplitude, predicted by both the APM and the (local) CfA data on $\xi(r)$, is $\simeq 400\ \Omega^{0.6}/b$ km s$^{-1}$ on scales less than $40\ h^{-1}$ Mpc and should be detectable in the current velocity surveys if $\Omega^{0.6}/b = 1$.

3. We calculate in detail the amplification in the cluster correlation function for clusters of various masses due to gravitational clustering assuming only that clusters of galaxies should be identified with regions with turnaround time less than the age of the universe. We use the data on both the slope of the cluster correlation function for Abell clusters of richness $\mathscr{R} \geq 1$, and on the dependence of the cluster correlation amplitde on the cluster richness/mass. Cluster masses for given $\mathscr{R}$ are normalized to Coma. We find that, for any value of $\Omega h$, CDM models cannot simultaneously fit data on the cluster correlation slope and amplitude, its amplitude-richness dependence, and the APM catalog data on $w(\theta)$. We show that using the data on the underlying galaxy correlation function, $\xi(r)$, at some fixed $r$ (we chose $r = 25\ h^{-1}$ Mpc), enables one to invert the amplitude-richness data to obtain the values of the rms fluctuations, $\Delta(M)/\Delta_8$, for the *pregalactic density field* on cluster mass scales. Applying the method to the data, we obtain the pregalactic density field, whose slope is in excellent agreement with the APM field on the same scales. Requiring then that the two amplitudes match fixes $\Omega$ to be 0.25–0.3 independently of the bias factor, the same value is implied by the dynamics of the Coma Cluster.

4. We then use the data on objects at high redshift to constrain the small-scale part of the pregalactic density field. We argue that data on the existence of clusters of galaxies at redshifts $\geq 1$–2, observations of galaxies at $z \sim 5$, and the recent determination of galaxy ages from Keck observations for a number of high-$z$ galaxies imply more power on small scales than predicted in CDM models normalized to the large-scale galaxy correlation data. We then reconstruct the pregalactic density field out of which modern-day (elliptical) galaxies have formed. To do this, we use the data on blue absolute luminosities of Faber et al. (1989) and assume the fundamental-plane relations to determine the initial halo mass (normalized further to reproduce the mass-to-light ratio of the Coma Cluster) and the X-ray data from *ROSAT* and *ASCA* to determine the halo velocity dispersion. Despite the simplifying assumptions, we recover a density field which is in good agreement with the simple extrapolation of the reconstructed density field from larger scales.

5. At the end of these steps we reconstruct the pregalactic density field over linear scales encompassing 2 orders of magnitude, $1\ h^{-1}$ Mpc $< r < 100\ h^{-1}$ Mpc. The recovered field is difficult to fit with CDM models and constant bias parameter over this range of scales. We argue that the most economical explanation of the density field on all scales would be to assume that the results in Figure 20 represent the pregalactic density field with constant bias parameter $b \simeq 1$ and

$\Omega \simeq 0.25$–$0.3$ as required by the dynamics of galaxy systems and the consistency between the X-ray observations of rich clusters and big bang nucleosynthesis (White et al. 1993).

I am grateful to the people who provided the data used in the paper: Sandy Faber for providing the absolute photometric data for galaxies, Kyoko Matsushita for permitting me to use the results from her thesis of *ASCA* observations of galaxies, Carlton Baugh for the data on the BE93 power spectrum, Mike Vogeley for the CfA data used for peculiar velocity calculations, and Will Sutherland for the APM data binned in six narrow magnitude slices. Particular thanks to Richard Mushotzky for several valuable discussions on X-ray observations of galaxies and to Raul Jimenez on the age determinations of high-redshift galaxies.

## REFERENCES

Abell, G., Corwin, H. G., & Ollowin, R. P. 1989, ApJS, 70, 1
Albrecht, A., & Stebbins, A. 1992, Phys. Rev. Lett., 68, 2121
Awaki, H., et al. 1994, PASJ, 46, L65
Bahcall, N. 1981, ApJ, 247, 787
Bahcall, N., & Soneria, R. 1983, ApJ, 270, 20
Bahcall, N., & West, M. 1992, ApJ, 392, 419
Bardeen, J., Bond, J. R., Kaiser, N., & Szalay, A. 1986, ApJ, 304, 15
Baugh, C., & Efstathiou, G. 1993, MNRAS, 265, 145 (BE93)
———. 1994, MNRAS, 267, 323
Begelman, M., & Rees, M. J. 1978, MNRAS, 185, 847
Bennett, C., et al. 1996, ApJ, 464, L1
Bertschinger, E., & Dekel, A. 1989, ApJ, 336, L5
Bertschinger, E., et al. 1990, ApJ, 364, 370
Blumenthal, G., et al. 1984, Nature, 311, 517
Bond, J. R., & Efstathiou, G. 1985, ApJ, 285, L45
Broadhurst, T., Ellis, R., & Glazebrook, K. 1992, Nature, 355, 55
Bruzual, G. 1983, ApJ, 273, 105
Cavalieri, A., & Szalay, A. 1986, ApJ, 311, 589
Cen, R., et al. 1992, ApJ, 399, L11
Chambers, K. C., & Charlot, S. 1990, ApJ, 348, L1
Chambers, K. C., et al. 1990, ApJ, 263, 21
Clutton-Brock, M., & Peebles, P. J. E. 1981, AJ, 86, 1115
Collins, C. A., Nichol, R. C., & Lumdsen, S. L. 1992, MNRAS, 254, 295
Da Costa, L. N., et al. 1994, ApJ, 437, L1
Davis, D. S., & White, R. E. 1996, ApJ, 470, L35
Davis, M., & Peebles, P. J. E. 1983, ApJ, 267, 465
Davis, M., et al. 1985, ApJ, 292, 371
Dekel, A., et al. 1993, ApJ, 412, 1
Deltorn, J.-M., et al. 1997, ApJ, 483, L21
Dey, A., et al. 1997, preprint
Dickinson, M. 1993, BAAS, 182, 6703.
Djorgovski, G., & Davis, M. 1987, ApJ, 313, 59
Djorgovski, G., et al. 1996, Nature, 382, 234
Dressler, A., et al. 1987a, ApJ, 313, 42
———. 1987b, ApJ, 313, L37
Dunlop, J., et al. 1996, Nature, 381, 581 (D96)
Eales, S. A., et al. 1993, ApJ, 409, 578
Efstathiou, G., & Rees, M. J. 1988, MNRAS, 230, 5P (ER88)
Efstathiou, G., Bond, J. R., & White, S. D. M. 1992, MNRAS, 258, 1
Efstathiou, G., et al. 1990, Nature, 348, 705
Eisenhardt, P., & Dickinson, M. 1992, ApJ, 399, L47
Faber, S., et al. 1989, ApJS, 69, 763
Fall, S. M., & Pei, Y. C. 1993, ApJ, 402, 479
Francis, P. J., et al. 1996, ApJ, 457, 490
Francis, P. J., Woodgate, B., & Danks, A. 1997, ApJ, 482, L25
Franx, M., et al. 1997, ApJ, 486, L75
Geller, M., & Huchra, J. 1989, Science, 246, 897
Giavalisco, M., Steidel, C. S., & Macchetto, F. D. 1996, ApJ, 470, 189
Gorski, K. 1988, ApJ, 332, L7
Gorski, K., et al. 1989, ApJ, 344, 1
———. 1996, ApJ, 464, L11
Gott, R., & Rees, M. J. 1975, A&A, 45, 365
Groth, E., & Peebles, P. J. E. 1977, ApJ, 217, 385
Groth, E., Juszkiewicz, R., & Ostriker, J. 1989, 346, 558
Haenhelt, M., & Rees, M. J. 1993, MNRAS, 263, 168
Hamilton, A., et al. 1991, ApJ, 374, L1
Hu, E. M., & Ridgway, S. E. 1994, AJ, 107, 1303
Hu, E. M., & McMahon, R. G. 1996, Nature, 382, 231
Jensen, L., & Szalay, A. 1986, ApJ, 305, L5
Jones, M. E., et al. 1997, ApJ, 479, L1
Juszkiewicz, R., & Yahil, A. 1989, ApJ, 346, L49
Kaiser, N. 1983, ApJ, 273, L17
———.1984, ApJ, 284, L9
———. 1987, MNRAS, 227, 1
Kashlinsky, A. 1982, MNRAS, 200, 585
———. 1987, ApJ, 317, 19
———. 1991a, ApJ, 383, L1
———. 1991b, ApJ, 376, L5
———. 1992a, ApJ, 399, L1 (K92)
———. 1992b, ApJ, 386, L37
———. 1993, ApJ, 406, L1 (K93)
Kashlinsky, A. 1994, in Evolution of the Universe and Its Observational Quest, ed. K. Sato (Tokyo: Universal Academy Press), 181
Kashlinsky, A., & Jimenez, R. 1997, ApJ, 474, L81 (KJ97)
Kashlinsky, A., & Jones, B. J. T. 1991, Nature, 349, 753
Kashlinsky, A., Tkachev, I., & Frieman, J. 1994, Phys. Rev. Lett., 73, 1582
Kent, S., & Gunn, J. 1981, AJ, 87, 945
Kochanek, C. 1996, ApJ, 466, 638
Lacy, M., et al. 1994, MNRAS, 271, 504
Lahav, O., et al. 1991, MNRAS, 251, 128
LeFevre, O., et al. 1996, ApJ, 471, L11
Lilly, S. 1988, ApJ, 333, 161
Limber, D. N. 1953, ApJ, 117, 134
Loveday, S., et al. 1992, ApJ, 390, 338
Lowenthal, J. D., et al. 1997, ApJ, 481, 673
Lucy, L. B. 1974, AJ, 79, 745
Lynden-Bell, D. 1967, MNRAS, 136, 101
Maddox, S., et al. 1990, MNRAS, 242, 43P (MESL)
Mahonen, P., Hara, T., & Miyoshi, S. J. 1995, ApJ, 454, L81
Mathewson, D., Ford, V. L., & Buchorn, M. 1992, ApJ, 389, L5
Matsumoto, H., et al. 1997, ApJ, 482, 133
Matsushita, K. 1997, Ph.D. thesis, Univ. Tokyo
Melott, A. 1992, ApJ, 393, L45
Narayan, R., & White, S. D. M. 1988, MNRAS, 231, 97P
Pascarelle, S. M., et al. 1996, ApJ, 456, L21
Peacock, J. 1991, MNRAS, 253, 1
Peacock, J., & Dodds, S. J. 1994, MNRAS, 267, 1020
Peebles, P. J. E. 1982, ApJ, 263, L1
———. 1980, Large-Scale Structure of the Universe (Princeton: Princeton Univ. Press)
———. 1987, Nature, 327, 210
———. 1988, in Large Scale Motions in the Universe: a Vatican Study Week, ed. V. C. Rubin & G. V. Coyne (Princeton: Princeton Univ. Press), 457
———. 1989, ApJ, 344, L53
———. 1990, ApJ, 362, 1
Perlmutter, S., et al. 1997, ApJ, 483, 565
Picard, A. 1991, ApJ, 368, L7
Politzer, H. D., & Wise, M. B. 1984, ApJ, 285, L1
Postman, M., & Lauer, T. R. 1995, ApJ, 440, 28
Postman, M., et al. 1986, AJ, 91, 1267
Press, W., & Schechter, P. 1974, ApJ, 187, 425
Rix, H.-W., et al. 1997, preprint (astro-ph/9702126)
Saunders, W., et al. 1991, Nature, 349, 32
Saunders, R., et al. 1997, ApJ, 479, L5
Schechter, P. 1976, ApJ, 203, 297
Schmidt, M., Schneider, D., & Gunn, J. 1991, in ASP Conf. Ser. 21, The Space Distribution of Quasars, ed. D. Crampton (San Francisco: ASP), 109
Schneider, D., Schmidt, M., & Gunn, J. 1991, AJ, 102, 837
Schneider, D., et al. 1992, PASP, 104, 678
———. 1994, AJ, 107, 880
Shaver, P. A., et al. 1996, Nature, 384, 439
Shaya, E., Peebles, P. J. E., & Tully, B. 1995, ApJ, 454, 15
Smoot, G., et al. 1992, ApJ, 396, L1
Steidel, C. S., et al. 1996, ApJ, 462, L17
Stompor, R., Gorski, K. M., & Banday, A. J. 1995, MNRAS, 277, 1225
Strauss, M., & Willick, J. A. 1995, Phys. Rep., 261, 271
Sutherland, W. 1988, MNRAS, 234, 159
Toth, G., Hollosi, J., & Szalay, A. 1989, ApJ, 344, 75
Trager, S. C., et al. 1997, ApJ, 485, 92
Turner, E. 1991, AJ, 101, 5
Van der Marel, R. P. 1991, MNRAS, 253, 710
Vittorio, N., Juszkiewicz, R., & Davis, M. 1987, Nature, 323, 132
Vittorio, N., & Silk, J. 1985, ApJ, 285, L39
Vogeley, M., et al. 1992, ApJ, 391, L5
Walker, T. P., et al. 1991, 376, 51
White, S. D. M., & Rees, M. J. 1978, MNRAS, 183, 341
White, S. D. M., et al. 1993, Nature, 366, 429
Willick, J. 1990, ApJ, 351, L5
Yoshii, Y., & Takahara, F. 1988, ApJ, 326, 1